Sandstone diagenesis in sediment-lava sequences: Exceptional examples of volcanically driven diagenetic compartmentalization in Dune Valley, Huab Outliers, NW Namibia.

Clayton Grove [1], Dougal A. Jerram[2, 3], Jon G. Gluyas[4], Richard J. Brown[4]

[1]Siccar Point Energy Limited, H1, Hill of Rubislaw, Aberdeen, AB15 6BY

[2]Centre for Earth Evolution and Dynamics (CEED), University of Oslo, 0316 Oslo, Norway

[3]DougalEARTH Ltd. Solihull, United Kingdom (www.dougalearth.com)

[4]Department of Earth Sciences, Durham University, DH1 3LE, United Kingdom

(E-mail: clayton.grove@siccarpointenergy.co.uk)

ABSTRACT

At the base of many flood basalt sequences and along volcanic rifted margins, volcanism can compete with the existing sedimentary environments, resulting in interbedded sequences of volcanic rocks and sediments. Here we report on sediment interlayers that are found in the lowermost volcanic units of the Etendeka flood basalts in NW Namibia (Twyfelfontein/Awahab Formations), part of the much larger Paraná-Etendeka Igneous Province. The sandstone bodies, predominantly eolian dunes, are isolated in a sequence of Lower Cretaceous (~ 134 Ma) lava flows. The upper most part or where sediment deposition and lava emplacement is observed to interact is characterized by barchanoid dunes, which were actively migrating during the emplacement of the lava flows. The fossil (isolated by lava) barchan dunes studied in "Dune Valley" show three characteristically different diagenetic styles. In Dune Valley, each dune body is completely encapsulated by lava, with additional igneous intrusions cutting through some bodies. We recognize three distinct styles of diagenesis: Type 1: Fossilised dunes that are red in color and lack major authigenic mineralization, with grain compaction and subsequent porosity loss being the dominant diagenetic process. Type 2: Dunes that have been bleached white, which have undergone a more complex diagenetic pathway. Type 2 dunes have abundant calcite, kaolinite, and böhmite as authigenic phases and lack hematite grain coatings. Detrital plagioclase is absent in white dunes (XRD analysis), with pseudomorphs of kaolinite common. This diagenetic assemblage results in the white dunes having lower porosity and permeability compared to the red dunes. The observations are probably due to a flux of carbon dioxide (CO_2), hydrogen sulfide (H_2S) and/or hydrogen (H_2) -rich hydrothermal groundwater derived from igneous intrusions below. Type 3: "Hot contact" effects at lava-flow contacts, where the unconsolidated dunes were rapidly indurated during lava emplacement (volcano-eogenesis). Type 3 diagenesis is restricted to << 1 m

depth below lava contacts and common in dunes displaying both Type 1 and Type 2 diagenesis. The distribution of diagenetic Types 1 and 2 is dune specific, and throughout Dune Valley approximately half of the dunes have been bleached (e.g, Type 2 diagenesis), whereas diagenetic Type 3 is a hot contact phenomenon and is therefore found along all basal lava and dike contacts. This work has relevance to understanding the development of sediment-lava systems, to hydrocarbon exploration and development in preserved sediment-lava sequences, and the hydrothermal process described provide an example of natural CO_2 sequestration.

INTRODUCTION

Sediment-lava interbeds are important as they have the potential to preserve features from paleoenvironments not usually recorded in the rock record, are targets for hydrocarbon exploration in volcanic margins, and provide detailed constraints on paleo-environment and burial effects in volcanism influenced basins. The most common examples of significant sediment-lava interbeds can be found in large-volume lava-flow fields, in volcanic margins, and in continental flood basalts. Sedimentary deposits that are partially or totally buried by volcanic rocks represent a transition or switching between sedimentary and volcanic environments. The eruption of lava flows and/or explosive units has the potential to quickly bury and interact with the sedimentary systems that are present at the time of their emplacement due to the overwhelming volumes of volcanic material erupted in relatively short time intervals (e.g, Peate et al. 2003; Ross et al. 2005; Jerram and Widdowson 2005; Bryan et al. 2010). The sedimentary systems present can be engulfed rapidly and preserved almost entirely by the lavas (e.g, Mountney et al. 1999a; Jerram et al. 2000a; Jerram and Stollhofen 2002; Petry et al. 2007). Where active sedimentation is contemporaneous with lava-flow emplacement, interbedded sediments and lava flows can develop. This can result in a complex spatial organization as sediments and lava dynamically interact and compete for accommodation (e.g, Jerram et al. 1999a; Jerram and Stollhofen 2002; Scherer 2002; Waichel et al. 2008; Waichel et al. 2011; Schofield and Jolley, 2013). Such mixed volcanic-sedimentary systems favor diagenesis not commonly found elsewhere, such as at hot lava-sediment contacts and authigenesis due to hot hydrothermal groundwater. Additionally, these sequences can be dissected by intrusions associated with the emplacement of the volcanic system, which can act as conduits to flow, modify the permeability system, compartmentalize the basin, and enhance hydrothermal activity (e.g, Schofield et al., 2015; Senger et al., 2017; Angkasa et al., 2017).

Offshore petroleum exploration has also highlighted the occurrence of similar isolated sandstone bodies within prospective hydrocarbon exploration areas in volcanic rifted margins worldwide (e.g, Jungslager 1999; Davison 1999; Schutter 2003; Smallwood et al. 2004). This raises additional questions about the petroleum reservoir potential of such sandstone bodies, the rock properties and diagenesis of the sandstones, and our understanding of the potential consequences of the volcanic processes on oil/gas-field development (e.g, Kudu (offshore Namibia), McLachlan 1990; Jerram et al. 1999a; Rosebank (UKCS), Helland-Hansen 2009; Schofield and Jolley 2013; Anne-Marie (Faroes), Beswetherick et al. 2009; Benbecula (UKCS), Hitchen et al. 2013). Currently knowledge is limited on the degree of igneous-related compartmentalization, to which igneous bodies

(intrusions or lava flows) contribute, and the role of volcanically induced diagenesis. It is also often unclear whether lava flows are in hydraulic connection with interbedded siliciclastic units, which may increase the overall reservoir volume of such units if they are, or make them less prospective if not. Clearly, an understanding of the development of sediment-lava stratigraphy and how its diagenetic history is recorded is of importance to understanding how these competing systems have interacted, with direct implications for reservoir characterization.

In order to investigate sediment/lava stratigraphy further, we describe the diagenetic fingerprint of hydrothermal activity on isolated sand bodies within a flood basalt pile, where contrasting diagenetic styles occur between discrete sand bodies that are separated by tens to hundreds of meters by lavas and igneous dikes. We test the hypothesis that the fluids responsible for differential diagenesis were spatially restricted by the igneous rocks, thereby compartmentalizing the groundwater flow regime.

Our results show that vertical and subvertical igneous intrusions are responsible for compartmentalizing the basalts and inter-basalt sediments (see also Rateau et al. 2013; Schofield et al. 2015; Senger et al., 2017) and the lava flows allow fluid movement between isolated sand bodies. Lava flows contain potential fluid pathways in vesicular, fractured, and brecciated regions, whereas the core regions of lava flows are more massive and potentially form barriers to flow where not fractured (e.g, Watton et al. 2014). In addition to reporting on fluid-flow compartmentalization using diagenetic fluids as a tracer, this contribution also describes how the diagenetic effects of these fluids have acted as a reservoir-degrading mechanism within the affected sand bodies (both porosity and permeability reduction). Further, the proposed mineral reaction is a natural example of the carbon dioxide sequestration mechanism of Hangx and Spiers (2009), such that a natural analogue to proposed CO_2 sequestration mechanisms has been identified in a mixed basalt-siliciclastic system (e.g, Jones et al., 2016). This has implications for the successful exploitation of similar systems for the long-term disposal of anthropogenic CO_2 (e.g, Matter et al. 2016). The discussion is directed to the early stages of diagenesis in sediment/lava interbedded sequences and contacts in the Paraná-Etendeka flood-basalt sequence, and its implications for understanding fluid flow and petroleum prospectivity in similar settings (e.g, inter-basalt and sub-basalt sediments in the Faroe-Shetland Basin, Rockall Trough, and inter-basalt sediments offshore Southern Atlantic, e.g, Brazil, Angola, and Namibia, as well as early volcanic sequences in flood basalts and volcanic margins globally).

CASE-STUDY OUTLINE AND GEOLOGICAL SETTING

97 The case study presented uses the Lower Cretaceous stratigraphy in NW Namibia (The Twyfelfontein and
98 Awahab Formations, about 134 Ma) (Mountney et al. 1998; Mountney et al. 1999a, 199b; Jerram et al. 1999a,
99 1999b; Jerram et al. 2000a, 2000b; Jerram and Stolhofen 2002; Dodd et al., 2015). These units represent an
100 exceptionally preserved example of where sediments have been buried and completely preserved within lava
101 sequences (e.g, Mountney et al. 1999a; Jerram et al. 2000a), with the lower parts of the Awahab formation
102 containing sandstone bodies which are isolated within the lava field (Jerram et al. 2000a). The rocks
103 (sandstones, volcaniclastics, basaltic lava flows) are cut by later dolerite dikes. The case study presented is in an
104 area named "Dune Valley" and is located in the foothills SW of Awahab (Mikberg) mountain, Huab Outliers,
105 Kunene Region, NW Namibia (Fig. 1). Desert exposure (70 % to nearly 100% outcrop) and nearly complete
106 preservation of lava-drowned barchanoid eolian dunes (Jerram et al. 2000a), now exhumed by preferential
107 erosion of basaltic lava, allow detailed sampling and mapping. Early diagenetic effects have been preserved due
108 to prolonged aridity (desert conditions have prevailed since the Cretaceous; e.g, Goudie and Eckardt 1999). The
109 arid Namibian setting contrasts with the South American correlative equivalent, the Botucatu and Serra Geral
110 Formations, where secondary diagenetic effects (large meteoric-water flux) in some cases have overprinted such
111 early features (e.g, França et al. 2003). Lack of exposure in South America makes detailed studies limited often
112 to quarries and coastal exposures (e.g, Petry et al. 2007, Waichel et al. 2008).

113 *Regional Geological Setting*

114 The term Huab Basin describes the basinal feature centered on the Huab River, containing sedimentary rocks of
115 the Palaeozoic–Mesozoic Karoo Supergroup and Mesozoic Etendeka Group (e.g, Horsthemke et al. 1990;
116 Jerram et al. 1999a; Mountney et al. 1999b), which rest on deformed Damaran basement rocks (500– 600 Ma)
117 (Fig. 2). The basin records the extensional tectonic regime and associated continental sediment deposition
118 relating to the breakup of Gondwana (Clemson et al. 1997; Jerram etal. 1999a), initially with deposition during
119 the Permian–Jurassic Karoo, followed by an erosional hiatus and subsequent Late Mesozoic rifting in the latest
120 Jurassic and Lower Cretaceous. The Huab Basin sedimentary rocks thin toward the south and lap onto the
121 Damaran basement, and clearly fill in a structurally bounded depression that roughly follows the present Huab
122 River (Mountney et al. 1999b). The study area (Figs. 1, 3) is situated within the Huab Outliers (Jerram et al.
123 1999a) south of the Huab River. The Huab Outliers preserve a complete section through the Huab Basin
124 sedimentary and volcanic sequence (Twyfelfontein and Awahab Formations).

125 The stratigraphic section of interest in this study is the transition from continental sedimentary rocks to
126 continental flood-basalt lava and crosscutting igneous intrusions (Fig. 2). This is marked by two formations: the
127 Twyfelfontain Formation and the Awahab Formation). The Twyfelfontain Formation was formerly known as
128 the Etjo/Cretaceous Etjo Formation (e.g, Horsthemke et al. 1990; Milner et al. 1995; Mountney et al. 1998;
129 Mountney et al. 1999a, 1999b; Jerram et al. 1999a, 1999b; Jerram et al. 2000a, 2000b). The current
130 Twyfelfontein Formation name was introduced by Stanistreet and Stollhofen (1999) and Schreiber (2006). In
131 this study, we use the term Twyfelfontain Formation as this clearly separates these Cretaceous rocks from the
132 Jurassic Etjo Formation rocks farther south in Namibia, and it is the current formation name used by the
133 Geological Survey of Namibia (cf. Schreiber 2006).

134 The Twyfelfontain Formation consists of predominantly eolian sedimentary rocks, occasional fluvial beds, and a
135 notable fluvial sandstone and conglomerate sequence at the base (known locally as "The Krone Member",
136 Mountney et al. 1998). The Awahab Formation is composed of interbedded sedimentary rocks (again
137 predominantly eolian) and lavas at the base, and thick lava sequences higher up (Milner et al. 1995; Jerram et al.
138 1999a) (Fig. 2). The lava stratigraphy has been subdivided based on geochemistry of the constituent lavas (e.g,
139 Milner et al. 1995; Jerram et al. 1999a). The lava stratigraphy is made up of olivine-rich lavas (low viscosity) at
140 the base, termed the Tafelkop lavas based on their geochemical type (Milner et al. 1995; Jerram et al. 1999a).
141 These then transition into basalts and basaltic andesites, termed the Tafelberg on geochemical type (Milner et al.
142 1995; Jerram et al. 1999a), and finally into silica-rich units (quartz latite) towards the top. In "Dune Valley" the
143 Tafelkop basalts are fed locally from dikes and the volcanic center called "Doros Crater", to the south. At the
144 time of eruption they built up a sizable shield volcano centered on Doros (Jerram et al, 1999a; Jerram and Robbe
145 2001; Marsh et al. 2001). The more voluminous Tafelberg type lavas onlapped and buried this shield volcano,
146 and mark the end of the preserved sediments in "Dune Valley" (Jerram et al. 1999a; Jerram and Robbe 2001).
147 These more voluminous lavas, covered the existing topography and peneplained the area prior to the almost
148 complete blanketing of the region with large-volume silicic eruptions (known locally as quartz latites; Milner et
149 al. 1995). The silicic units mark the upper parts of the stratigraphy in this area and extend into the Paraná Basin
150 (Bryan et al. 2010). Within Dune Valley, the Twyfelfontein Sandstone is predominantly buried by Tafelkop-
151 type lava, which, in this location, is morphologically a compound-type lava (cf. Walker 1971; Jerram 2002),
152 with minor sediment in contact with Tafelberg-type basalts (massive inflated sheet and tabular flows) towards
153 the top of the sequence. Throughout the sequence, sills, dikes, and shallow intrusions are found associated with
154 the emplacement of the Paraná-Etendeka province in the Lower Cretaceous.

Lava-Sediment Interaction

At the onset of effusive volcanic activity, marking the start of the Parana-Etendeka igneous province, the Twyfelfontein erg system (in Dune Valley) was sequentially buried with pahoehoe lava of Tafelkop type. The lava flows passively drowned the dunes as they inflated and filled in the topography (Jerram et al. 2000a). This resulted in the preservation of eolian features with very little disturbance (e.g, dune forms and topset beds) (Jerram et al. 1999b, Jerram et al. 2000a), the process is summarized in Figure 4 (modified from Jerram et al. 1999b). Initially the desert contained large draa dune forms over 100 m high in places (Mountney et el. 1999a), as part of the large desert sand sea (erg) system prevailing across the Paraná-Etendeka basins at the time (Jerram et al. 2000a; Scherer and Goldberg 2007). Sand mobility, and volumes of available sand, were restricted by successive burial by lava flows, such that second- and- third generation dunes resting on lava surfaces were sediment starved, were reduced in overall thickness, and became barchanoid in shape in the upper parts of the system (e.g, Mountney et al. 1998; Jerram et al. 2000a). Adjacent dunes were separated by distances of c. 100 m during lava inundation (Figs. 3, 5, 6). When drowned by volcanic activity the barchans were hence completely encapsulated by lava.

METHODS

The distribution of sand bodies within the lava sequences in Dune Valley was mapped out along with the main types of diagenetic coloration, as seen in the field (Figs. 3 and 5). Once the outcrops were characterized, samples were taken for further detailed analysis. A total of 23, 30-μm-thick, blue-resin-impregnated thin sections, which were stained for potassium feldspar (HF etched and sodium cobaltinitrite treated) and carbonate (alizarin red and potassium ferricyanide) were prepared and modal abundances of minerals measured using standard point-counting techniques (500 points, see Grove and Jerram 2011 for uncertainty analysis), and studied under both plane-polarized and cross polarized light. Chips from the 23 samples were also inspected using a Hitachi TM1000 scanning electron microscope (SEM). Five samples were lightly crushed and analyzed as an oriented powder on glass slides using a Bruker D7 X-Ray diffractometer using Cu K-alpha 1 radiation (1.5406 Å). Calcite cements were identified in thin section using cathode luminescence and staining techniques (e.g, alizarin red and potassium ferricyanide). Measurements of $\delta^{13}C$ and $\delta^{18}O$ values were made at Durham University on four samples of calcite and corrected to international reference standards (including NBS 19 and NBS 18 calcite). Stable-isotope data for calcite are presented relative to VPDB. Five samples were analyzed for major elements using a Panalytical PW2404 wavelength-dispersive sequential X-ray spectrometer at the

University of Edinburgh. Permeability measurements were taken on 20 samples using a probe permeameter at the University of Aberdeen (e.g, Hurst and Goggin 1995), held in a clamp. Multiple measurements were carried out on each sample (up to 19) unless permeability recorded 0 md after several attempts. Permeability was also measured on four 26 mm core plugs (also measured with the probe permeameter) using a Frank Jones Hasler sleeve-type porosimeter with a confining pressure of 400 psi (2.8 MPa) at the University of Aberdeen. Porosity was calculated as total optical porosity from thin-section analysis (by point counting). As a control, sample NG52 was collected from the major erg (equivalent normal red sand, Type 1) tens of meters away from any igneous contacts and does not display any diagenesis related to igneous activity.

DIAGENESIS

Petrology and Mineralogy

Three types of diagenesis are identified in the sandstones, and are petrographically and mineralogically described in detail below. They can be found in the isolated sand bodies in "Dune Valley" and also in the major and minor erg units (e.g, Jerram et al. 1999a), which are found stratigraphically below the lava-interbedded isolated dunes. "Type 1" diagenesis is found in red isolated dunes, and red areas of the main and minor erg system. "Type 2" diagenesis is found in white isolated dunes, and in patches within the main and minor erg system. Both red and white isolated dunes display "Type 3" diagenesis near to hot lava contacts, with no appreciable difference between red or white isolated dune contact zones, as well as on the hot-lava/sediment contacts in the major and minor erg units (e.g, Jerram and Stollhofen 2002). The three types of diagenesis and how they are manifest in the sandstones are described in detail in the following sections, concentrating first on the key observations for each, then a short discussion about the diagenesis types, before a broader discussion on the implications for understanding the main controls on diagenesis and fluid flow.

Type 1 Diagenesis Observations- Burial Diagenesis

Type 1 diagenesis represents the normal burial-related diagenesis, without the influence of the igneous system. This burial diagenesis is exhibited in the isolated red dunes, where the original mineralogy has not been overprinted by igneous-related affects. Isolated red dunes are compacted subarkosic litharenites. They are composed of rounded eolian grains in well sorted grain-flow lamellae (fine to coarse sand) and less well sorted, rounded to subrounded grain fall (very fine to fine sand) lamellae (e.g, Howell and Mountney 2001). The detrital grains comprise quartz, potassium feldspar, plagioclase, lithic grains, and opaque minerals (ilmenite)

212 (Table. 1). Ilmenite is not widely disseminated and appears to form small placer deposits controlled by grain
213 density. Detrital grains are coated with hematite, which gives the red coloration (Figs. 7C, 8A). Here sutured
214 quartz grains suggest compaction through quartz dissolution; this appears to have been one of the main
215 diagenetic processes (e.g, Fig. 7C sutured grains). Cements are rare, although occasional quartz overgrowths are
216 present on some grains (~ 1.5%). Crushed potassium feldspar grains exhibiting shear and dilation along
217 cleavage planes were also observed consistent with the work of Dickinson and Milliken (1995), who initially
218 described the formation diagenesis. Porosity averages 15.2% in Type 1 sandstone and permeability averages
219 1095 md.

220 In the present study "Dune B" (Figs. 3, 5, 6) has been chosen as the type example of Type 1 diagenesis because
221 of its superior vertical exposure (2.5 m) allowing excellent access. It should be noted that "Dune B" can be
222 found only 120 m south of "Dune A" (a white dune) (Fig. 5), and in close proximity to many other isolated
223 dunes which are white. In the field, Type 1 dunes are clearly identified compared to Type 2 dunes based on this
224 red or white color (e.g, Fig. 5). Red sand is also dominant in the minor and major erg units, stratigraphically
225 below (Fig. 2), separated by lava (e.g, Jerram et al. 1999b).

226 *Type 2 Diagenesis Observations- Isolated White Dunes*

227 White (yellow or white in weathered outcrop) sandstones are distributed throughout the Twyfelfontein
228 Formation, and where they occur as isolated dunes due to flooding by lavas (Fig. 4), there appears to be no
229 intrinsic pattern to their distribution, occurring with red isolated dunes in close proximity (Fig. 5A, C). At
230 outcrop scale, the only difference appears to be color, with sedimentary structure showing no difference in
231 morphology (e.g, Fig. 5B, C). It can be shown that the white dunes were deposited in the same way as the red
232 dunes as isolated migrating barchanoid dunes which were preserved by burial under lava flows (e.g, Mountney
233 et al. 1998; Jerram et al. 2000b). The question then arises regarding the diagenetic history of these white
234 sandstones, and how it differs from the red eolian units.

235 Thin sections of the white sandstone indicate that it is also a subarkosic litharenite. Rounded to subrounded
236 quartz grains occur in grain-fall and grain-flow lamellae, which are usually well sorted. Detrital grains are
237 similar to those in the red dunes. However, feldspar grains are visibly corroded or are completely replaced by
238 clay. Plagioclase feldspar grains show the most intense alteration, with no petrographically identifiable grains
239 being encountered under optical microscopy that could be identified based on albite twinning. Any plagioclase
240 encountered was identified based on lack of yellow staining from sodium cobaltinitrite and by ruling out

identification as quartz (crossed-polars examination); therefore plagioclase has probably been petrographically overestimated (Table 1; Appendix 1); most counted plagioclase grains are probably in fact completely kaolinitized pseudomorphs (SEM analysis confirms this). Potassium feldspars in white sandstone samples are also frequently corroded or partially transformed into clay minerals (Fig. 8B). Hematite grain coatings are absent in the white sandstone, but opaque detrital minerals are still present, as are occasional aggregates of hematite in pore spaces (this may be a later oxidation product of pyrite). The assemblage of authigenic minerals is different from that of the red dunes and can be classified using petrographic techniques. Under the petrographic microscope the assemblage is composed of kaolinite, calcite, and occasional quartz overgrowths. Calcite and kaolinite are usually associated, and both replace feldspars and fill pore space. Porosity in Type 2 sandstone is lower than the Type 1 sandstone, averaging 4.8%. Permeability values in the white sandstone increase from negligible values in the Type 3 (see below) contact zone, but do not exceed 44 md (Figs. 9, 10), with an average of 26 md.

SEM examination of the samples confirmed the identified assemblage from light microscopy and enabled the additional identification of pore-lining böhmite (as pisolitic aggregates (Fig. 11), cf. Wu et al. 2012; Cai et al. 2009). Böhmite proved to be a common lining of pores in the white sandstone under the SEM, with all white samples having the mineral in abundance. It is not clear if there are any specific trends of böhmite throughout the dunes due to its difficulty to detect and quantify with optical microscopy. Kaolinite can be seen in SEM to form books that fill pore space and aggregates that replace feldspars (e.g, Fig. 11D). Calcite in SEM is always found to be associated with kaolinite and frequently fills pores (Fig. 11A).

X-ray diffraction analysis was performed on sample NG29, which comes from 3 m below the hot contact in isolated white Dune A (Fig. 12). This distance is significantly outside the ~ 30 cm contact zone where Type 3 diagenesis occurs. The spectrum for NG 29 was compared with NG32 isolated red Dune B, 2 m below the contact (limited by outcrop exposure). The white sandstone did not display any plagioclase peaks (e.g, anorthite 100 peak, 3.19 Å (27.96° 2θ)) and orthoclase peaks were weakened. Kaolinite (7.17 Å (12.35 ° 2θ) and 3.58 Å (24.83 ° 2θ) peaks are present in the white sand (not found in the red sand). Böhmite was not detected in XRD, despite it being an obvious phase in SEM. This is probably due to its low volume abundance. Calcite did not show a clear spike, despite being seen in optical microscopy and SEM.

Given that all of the isolated dunes were deposited at the same stratigraphic level and subsequently either bleached white or not, it is instructive to determine how the two main types of diagenesis in the dunes evolved

and whether there has been any net flux of elements in or out of each system. X-ray fluorescence analyses were performed on five samples with the aim of testing enrichment or depletion in elements as a result of dune bleaching- specifically, to test the hypothesis that there was depletion in relative iron abundance in white dune sandstones. For analysis, the data were normalized to NG52, which is considered to be background red sandstone. The geochemical differences between red and white dunes (Fig. 13A) support the petrographic observations. Iron and sodium are depleted in white dunes compared with NG52 and NG32. Calcium is enriched in the white sample, and LOI is ~ 7 times that of NG52. Aluminum is approximately equal in Type 1 and Type 2 sandstones.

Type 3 Diagenesis Observations- Hot Lava Contacts

The upper surfaces of fossil dunes in the study area often display features such as topset beds and eolian ripples, as well as preserved lava-emplacement features such as striations and lava imprints (see Jerram et al. 1999a; Jerram et al. 2000a; Jerram and Stollhofen 2002 for description). These features indicate that the upper dune surface was contemporaneous with and covered by flowing lava. Type 3 diagenesis is found only in these upper dune surfaces. Basal surfaces (i.e, cold contacts: sands that were deposited on top of the solid cooled upper surface of lava) usually display Type 1 or Type 2 depending on overall dune diagenetic type. Generally, there is no evidence of significant early weathering of the cooled-lava top surfaces, indicating that little time passed between the emplacement of the lava and migration of sand dunes (Jerram and Stollhofen 2002).

For both Dune A (NG26) and Dune B (NG31) contacts, porosity is always found to decrease towards the formerly hot contact (Fig. 9 A). Reductions in porosity in the sandstones start to become apparent at depths of < 2 m from the contact with the base of lavas. At these depths porosity values are 15–20%, and they decrease to < 1% at the contacts with the lava. Permeability in red dunes increases rapidly away from the contact, reaching background permeability of between 100 md and 1000 md at depths of ~ 30 cm below the once-hot lava contact. At hot-lava contact zones, permeability approaches negligible values (Fig. 10 A). Permeability in white dunes does not return to these normal background values outside of the contact zone, due to Type 2 diagenesis.

The modal proportion of authigenic calcite and authigenic clay (chlorite identified, other clays undifferentiated) increase toward hot contacts (Figs. 7, and 14). In red sandstones, clay increase is apparent only at the contact. Porosity loss in the sediments occurred through both compaction and mineral authigenesis, as is shown by the porosity loss measurements (COPL % and CEPL %) (see Appendix. 1). In both dune types the proportions of opaque minerals (mainly hematite and goethite rims on detrital grains) increase slightly toward hot contacts;

importantly, both red and white dunes have high abundance of opaque mineral near the hot lava contact. Calcite increases towards lava contacts in red dunes but does not in white dunes. Compactional porosity loss, calculated using the method from Lundegard (1992), increases towards contacts (between ~ 30 cm and the contact (Fig. 9B)). Cementational porosity loss (Lundegard 1992) shows more variation but is highest near contacts. Detrital mineralogy shows little variation with proximity to hot contacts (red dunes).

The results of the X-ray diffraction are summarized in Table. 2; the data generally confirm the petrographic observations (Fig. 7). Both red and white dune contacts produce strong calcite peaks at 3.035 Å (~ 29.46° 2θ). NG 31 produced a peak at 3.15 Å (28.3 ° 2θ) that corresponds to fluorite; this supports a tentative petrographic identification of this mineral. Fluorite pore fills are also occasionally found in the Twyfelfontein Formation elsewhere under other hot contacts. NG26 produced clay peaks at 7.17 Å (12.35 ° 2θ) and 3.58 Å (24.83 ° 2θ); the strength of the 3.58 Å peak supports the interpretation of clinochlore as the clay phase, but kaolinite is also possible. Hematite was not detected with XRD, possibly due to its presence in very low abundances (petrographic observations overestimating its abundance).

In samples from hot contacts (Type 3) (Fig. 13 B) both samples (red and white dunes) are geochemically similar with the exception of manganese, which may relate to the presence of Ilmenite. Both contacts are enriched in magnesium and calcium, and show minor enrichment in iron. LOI is also higher than NG52, which is an indication of the presence of the release of trapped volatiles (H_2O and CO_2) during ignition, probably from within the clay minerals and carbonate. Note that the enrichment in calcium is ~ 27 times that of NG52. Basaltic rocks can contain up to 25% by weight of calcium, magnesium, and iron (Matter et al. 2016).

Stable-Isotope Analysis of Calcite Cements (Type 2 and Type 3 Diagenesis)

Only samples containing calcite could be analysed; therefore there are stable-isotope data only for Type 2 and Type 3 sandstone, Type 1 not having any calcite. Three samples from Type 2 (white) and one sample from Type 3 returned an adequate CO_2 yield for stable-isotope analysis. When $\delta^{13}C$ is plotted against $\delta^{18}O$, the Type 2 (white) sandstone calcite forms a field separate from Type 3 diagenesis calcite (Fig. 15A). $\delta^{18}O$ and $\delta^{13}C$ are heavier for Type 2 calcite ($\delta^{18}O$ mean = -2.9‰ V-PDB, $\delta^{13}C$ mean = -0.6‰ V-PDB) than for Type 3 calcite ($\delta^{18}O$ mean = -13.6‰ V-PDB, $\delta^{13}C$ mean = -9.3‰ V-PDB.

In order to understand the origin of the Type 2 and Type 3 calcite, modelling was performed to test what water temperature and water compositions could produce the observed calcite compositions. The models were set up

using a range of water compositions: Cretaceous meteoric water in Namibia ($\delta^{18}O \approx -4.7$ to -5.1‰ SMOW) (see below for estimation method) and magmatic water ($\delta^{18}O$ 7‰ SMOW to 13‰ SMOW, Brownlow, 1996). Fractionation constants A = -3.39 and B = 2.78 (O'Neil et al. 1969) were used. The composition of meteoric water in Lower Cretaceous during the Etendeka volcanism was estimated by taking the Lower Cretaceous Namibia palaeolatitude of 29º to 32º south from Scotese (2001) and the variation of $\delta^{18}O$ with latitude from Bowen and Wilkinson (2002).

The model for Type 2 calcite (Fig. 15B) shows the Lower Cretaceous meteoric water would precipitate calcite with the observed values at temperatures between 20 °C and < 0º C. When magmatic values for water are modelled, temperatures required are between 50 °C and 150 °C.

The model for Type 3 calcite (NG31) (Fig. 15B) shows that precipitation from Lower Cretaceous meteoric water would have been at temperatures between 50 °C and 60 °C. Magmatic waters would have precipitated calcite at temperatures between 180°C and 330°C.

The modelled temperatures for Type 3 calcite are consistently hotter than Type 2 calcite, consistent with the hypothesis that the Type 3 calcites were eogenetic, formed during lava cooling at the hot lava-substrate contact. The Type 2 calcites show low temperatures that are not consistent with precipitation from a meteoric aquifer given the observed mineral assemblage association and the likely aquifer temperature in a hot, arid setting. For instance, the present-day aquifer temperature around the study area in Namibia is > 25 °C at even shallow depths (20-50 m) (Marx, 2009). More realistic temperatures are possible when the water is enriched with O^{18} over that of the predicted meteoric water. A possible-magmatic water component of the aquifer is therefore supported, and the aquifer could have comprised meteoric water, enriched by a magmatic-water component sourced from degassing igneous intrusions. The Type 3 calcite precipitated before the Type 2 calcite (both red and white dunes have Type 3), and therefore if precipitated in the subsurface should show cooler temperatures reflecting shallower burial (assuming normal burial). However, the temperatures modelled are hotter. This suggests that meteoric water is unlikely because if both were precipitated in the subsurface within a meteoric water derived aquifer during normal burial, the earlier cement would show lower temperatures, which is opposite to the observation. The temperatures modelled from magmatic waters are achievable at the contact with a basalt lava flow (c. 1200º C). Therefore, a magmatic origin of the Type 3 calcite is suggested.

The $\delta^{18}O$ and $\delta^{13}C$ values for the calcites for Type 2 and Type 3 calcites are compared with other calcites in Figure 15A. Neither calcite in this study directly overlies any of the fields chosen from the literature. The Type

3 calcite plots closer to the high-temperature geothermal calcites than Type 2, reflecting its higher-temperature origin from possible magmatic volatiles. The Type 3 calcite is isotopically light, similar to what would be expected for either a magmatic carbon or a biologically derived carbon. Figure 15A (fields 10 and 11) shows that calcretes formed under biological influence plot distinctly from the Type 3 calcite, supporting a magmatic rather than a biological origin. Further, no evidence of vegetation (e.g, fossil roots) has been found in the Twyfelfontein Formation. The Type 2 calcite plots closest to the geodes in the Paranã Basalts from Brazil (Gilg et al. 2003) and calcites found in sedimentary beds associated with Jurassic basalts in Namibia (Gierlowski-Kordesch et al, 2015), supporting the igneous association. Both the red and the bleached sandstones of the Navajo and Entrada Sandstone Formations (Chan et al, 2000; Garden et al, 2001; Beitler et al, 2005) are plotted in Figure 15A, none of which overlie the Type 2 white sandstone calcite in the Twyfelfontein Formation, supporting the hypothesis that the origin of the bleaching is different from the hydrocarbon-migration-related process observed in the Navajo and Entrada Formations.

In summary, the stable-isotope data suggest that the Type 3 calcite formed under hot conditions, with oxygen and carbon of a likely magmatic origin and that the Type 3 calcite formed in an aquifer with meteoric and magmatic components under cooler conditions, likely between ~ 25º C and 150º C.

Type 1 Diagenesis- Discussion of Burial Diagenesis

Dickinson and Milliken (1995), who first described the sandstone diagenesis in the Huab area, concentrated on the sandstones beneath the lava flows and made no distinction between the different red or white diagenesis types or indurated sediment found at the hot lava contacts. They readily observed features associated with burial diagenesis and deformation of grains, but they concluded that the conditions under which brittle deformation occurred in the sandstone were poorly constrained because the burial history is uncertain. Dickinson and Milliken (1995) principally investigated the role of brittle deformation and pressure solution away from the igneous affected sandstones and therefore did not describe the white sandstone or the lava-sediment contacts; their study can be taken as a good description of the Type 1 diagenesis.

It is clear that there has been significant erosion of the original lava sequence to expose the stratigraphy in the Huab Basin, although the exact extent and thickness of the original volcanic stratigraphy in flood basalts is notoriously difficult to estimate (e.g, Jerram and Widdowson, 2005). The overall thickness of the Paranã - Etendeka lavas, and thus the potential depth of subsequent burial, has been estimated to be as thick as 3-4 km based on the overall Paranã -Etendeka stratigraphy (e.g, Peate 1997) and from apatite fission-track analysis (e.g,

Raab et al. 2005). Although such estimates contain a significant error, it is likely that the sandstones considered in the present study have suffered some burial diagenesis under a significant overburden of volcanic stratigraphy. We propose that Type 1 diagenesis seen in the red sandstones is a function solely of this burial diagenesis and represents sandstone that has not been subjected to any hot-contact diagenesis (Type 3) or to a flux of fluid that was responsible for Type 2 diagenesis.

Type 2 Diagenesis- Discussion of Isolated White Dunes

Porosity reduction due to compaction processes visually appears more intense in thin sections of the white sandstone than in the red sandstone (e.g, thin-section photomicrographs in Fig. 8A. vs. in Fig. 8B; porosity values in Fig. 9). Increased visual compaction may have resulted from the weakening of feldspar grains during dissolution. These grains were then deformed to fill adjacent pores, or dissolved, thus reducing matrix strength. When quantified however, COPL is not significantly different in red or white dunes (Fig. 9). Figure 9 shows that it is cementation (CEPL) that contributes most to the additional porosity loss. Figure 10B shows a clear separation between the Type 1 and Type 2 diagenesis in the permeability-porosity cross plot, with little overlap, despite relative position in the isolated dunes being approximately equal.

Modal analysis of thin sections indicates that the white dunes have up to four times the amount of clay and five times the amount of calcite as the red dunes (Fig. 14D). Authigenic calcite shows no correlation with distance below lava in the white dunes. The white dunes contain both calcite generated during the emplacement at hot contacts and calcite formed during bleaching. Conversely, there is a negative correlation in red dunes between calcite and distance below the lava, as calcite here is controlled solely by Type 3 diagenesis in the absence of Type 2 diagenesis.

Authigenic quartz occurs in slightly lower abundance in white dunes and shows significant variability and no correlation with distance below the lava. The lower abundance of authigenic quartz may be due to pore-lining clay minerals inhibiting quartz precipitation during further burial, compared to the clay-absent red sandstone. Opaque minerals are less abundant in the white sandstone (the hematite grain coating being absent) and show a weak negative correlation with distance below lava, due to the Type 3 diagenesis at the contact (locked-in hematite); in the red sandstone, opaque minerals show no correlation with distance (Fig. 14C). The difference between the abundances of authigenic minerals has been tested using the statistical “Students T-Test” (e.g, Hazewinkel 2001). The results from this show that porosity, permeability, and abundances of authigenic quartz, authigenic calcite, and authigenic clay are statistically (at the 95% level or greater) different between red and

414 white dunes (Table. 3). Abundance of opaque minerals was not found to be statistically different. This is
415 because the hematite was probably being redistributed from grain coatings to the identified pore-filling
416 aggregates, noted also as iron oxide nodules in outcrop. The likely process is reduction of hematite grain
417 coatings and reprecipitation as pyrite nodules, which are oxidized during exhumation into hematite.

418 The interpretation of the geochemistry suggests that a flux of fluid must have been necessary to allow
419 enrichment and depletions in elements. If feldspars were simply transformed into the authigenic minerals, with
420 no loss or gain from the system, the bulk rock would be similar to NG52. Importantly, the loss of sodium in the
421 white dune shows that only the calcium from dissolving plagioclase was being completely sequestered into
422 authigenic minerals (otherwise sodium would mirror calcium). No sodium-containing authigenic minerals were
423 found in quantity, sodium being mobile in groundwater (White 1957). The sodium was probably transported out
424 of the system in solution; it should be noted that sodium is commonly found at elevated concentrations in
425 thermal springs of volcanic origin (White 1957). Aluminum is conserved, presumably being rapidly
426 incorporated into böhmite and kaolinite. The calcium enrichment suggests that calcium was being transported
427 from elsewhere in the system and being precipitated in white Dune A. A possible source for this calcium is other
428 sand bodies being depleted or volcanic glass and/or plagioclase in lavas part of the volcanic pile. Interaction
429 with the lavas in the pile is also consistent with the possibility of basalt-water interaction enriching the
430 hydrothermal water in heavy oxygen and is supported by the observation that the Tafelkop basalts are vesicular,
431 hence probably permeable. High LOI confirms that NG29 is rich in hydrated minerals (clays) compared to
432 NG52. Note that the depletion of iron in the white sandstone is minor, possibly as a function of the low original
433 iron concentration, but more likely supporting the hypothesis that iron was being locally redistributed into
434 nodules, with only a minor amount leaving the system.

435 These observations together depict a system in the isolated white dunes where hematite was being dissolved
436 from grain rims, and böhmite, kaolinite, and calcite were being formed at the expense of feldspar. These mineral
437 transformations resulted in bleached and compacted sandstone, with reduced primary porosity.

438 *Type 3 Diagenesis- Discussion of Hot Lava Contacts*

439 The observations of Type 3 diagenesis support the interpretation that contact diagenesis was an early-stage
440 phenomenon, during emplacement and cooling of the lava. This is also supported by Type 1 and Type 2
441 diagenesis not affecting upper-contact-zone sediments in dunes that have been affected by Type 3 diagenesis.
442 This variation in diagenesis was initially described as “hot contact” diagenesis (Jerram and Stollhofen 2002). It

443 is proposed that when the lava was emplaced onto the eolian sand substrate, volatiles would have been
444 degassing (likely components include water, carbon dioxide, chlorine, fluorine, sulfur dioxide, hydrogen sulfide
445 and carbon monoxide as major components (e.g, Delmelle and Stix 2000; Lowenstern 2001; Simmons and
446 Christenson 1994; Shevenell and Goff 1993; White 1957), flowing following a pressure gradient towards
447 atmospheric pressure. H_2O is the most common volcanic gas, followed by CO_2, although in gases liberated from
448 basaltic magmas CO_2 sometimes exceeds water (Lowenstern 2001). During ascent of the magma to eruption,
449 CO_2 begins to exsolve before H_2O because of lower solubility in magma and remains as a low-density vapor
450 phase (Lowenstern 2001) as vapor filled vesicles in the molten magma. As the magma ascends to shallow
451 depths (1–4 km) H_2O and CO_2 degassing is forced (Lowenstern 2001). Erupting magma should then contain
452 vesicles comprising vapor-phase volcanic gas, dominated by CO_2 and H_2O, with proportions dependent on rate
453 of ascent. Most of these volatiles are released into the atmosphere during eruption (e.g, a fire fountain). The
454 stable-isotope evidence from Type 3 diagenetic carbonates, however, suggests that lava flows must still contain
455 enough magmatic CO_2 (vapor phase vesicles) at the time of emplacement to form the observed cements. We
456 propose the following mechanism for the presence of magmatic CO_2 in the immediately sub-basalt sand: The
457 pore space in the unconsolidated sand would have been at atmospheric pressure, so when the newly emplaced
458 lava cooled, a proportion of the gases would have invaded the pore space (driven by pressure gradient) and
459 reacted with the sand. This occurred with feldspar first (supported petrographically by the apparent increase in
460 feldspar breakdown to clays). Feldspar decomposition would have reduced feldspar strength, facilitating
461 mechanical compaction by rearrangement of grains. Note that the increased compaction is not apparent farther
462 than ~ 30 cm below the contact. Remaining porosity was filled by calcite, with carbon being sourced from
463 degassed magmatic CO_2 and calcium being sourced from reacting volcanic glass and plagioclase (igneous and
464 detrital). Mild hydrothermal activity is therefore inferred to have existed around the contact (in modern settings
465 this would be manifested on the lava surface as steaming fumarole vents). These observations are consistent
466 with the "hot" contacts seen between the lowermost lavas and both the major and minor erg sediments (Jerram
467 et al. 1999b; Jerram and Stolhofen 2002). This suggests that, if indeed the contact effects described are eogenic
468 (early diagenesis) as proposed, a low-porosity and low-permeability cap to individual isolated dunes would have
469 been formed, before any significant burial (and therefore Type 1 or more importantly Type 2 diagenesis). There
470 is also evidence for former hydrothermal activity during lava emplacement in the form of a fossil fumarolic
471 pipe, which was found where lava bulldozed into the sand as an invasive flow, and subsequently degassed
472 through the loose sand above. The XRF analysis suggests elemental flux into the system (magnesium and

calcium). We infer that enriched magnesium and calcium are hosted in the calcite cement and iron and magnesium are in the chlorite. If the elements were simply redistributed from feldspars during the Type 3 diagenesis, there should be no enrichment in these elements. It is therefore proposed that calcium, magnesium, and iron are at least partially sourced from the overlying lava, probably during cooling and hydrothermal decomposition of volcanic glass.

UNDERSTANDING THE MAIN DIAGENTIC CONTROLS

Most of the volume of the intra-lava sediments in this study are affected by either Type 1(burial diagenesis, red sandstone) or Type 2 (white sandstone) diagenesis, with Type 3 diagenesis volumetrically minor, restricted to relatively thin contact zones. What is driving this variation? The petrographical, mineralogical, and geochemical differences between isolated red dunes (Type 1 diagenesis) and isolated white dunes (Type 2 diagenesis) have been established. Chemical bleaching of sandstones is not rare; it has been documented elsewhere, commonly as a result of hydrocarbon migration through sandstone (Moulton 1926; Surdam et al. 1993; Kirkland et al. 1995; Parry et al. 2004; Schöner and Gaupp 2005; Ma et al. 2007). Bleached zones have been used to indicate migration pathways of hydrocarbons and to infer the existence of emptied reservoirs (Kirkland et al. 1995; Beitler et al. 2003; Beitler et al. 2005).

Where hydrocarbons have migrated through red sandstones, the bleaching has been attributed to acidic, reducing conditions (e.g, Ma et al. 2007; Surdam et al. 1993). These conditions can be achieved by biologically mediated oxidation of CH_4 to produce CO_2 and simultaneous reduction of SO_4^{2-} to H_2S (Kirkland et al. 1995). In such a reaction, the CO_2 and H_2S are achieved in conditions where dissolved H_2S (present as HS^-) reacts with ferric iron oxide (hematite) to form soluble ferrous iron. The HCO_3^- reacts with Ca^{2+} and Mg^{2+} to form carbonate minerals (Surdam et al. 1993; Kirkland et al. 1995). Dissolved ferrous iron and H_2S would not necessarily react immediately to precipitate as iron minerals (e.g, pyrite) and can migrate in pore waters (Kirkland et al. 1995). These conditions could also be achieved without contemporary biological mediation, as many hydrocarbons are associated with H_2S and CO_2. A petrographic study of bleached sandstones has documented alteration of feldspars to clay (kaolinite) in these settings (Ma et al. 2007).

The migration of hydrocarbons is an unlikely mechanism for the bleaching (Type 2 diagenesis) of the sandstones in the study area because (A) there is no significant source rock in the thin underlying Karoo sequence this far south in the Huab Basin, and (B) hydrocarbon residues have not been observed in the field or during subsequent petrographic studies (including with UV light). However, the same chemical species required

(H_2S and CO_2) can be generated by magmatic degassing (e.g, Henley and Ellis 1983; Rye 2005; Delmelle and Stix 2000), probably during magma solidification (Arnórsson 1986) and are common in hydrothermal systems (e.g, White 1957; Henley and Ellis 1983). We infer that the fluids that passed through the isolated dunes of the Twyfelfontein Formation were hydrothermal in origin and were enriched in magmatic gases originating from degassing mafic intrusions at depth. It should be noted that many dolerite sills and dikes can be found in the area (e.g, Marsh et al. 1991; Duncan et al. 1989; maps presented in this study).

Our observations test this hypothesis. Firstly, both red and white isolated dunes were deposited at similar or the same stratigraphic levels, and have identical detrital compositions; this is illustrated by the fact that the Type 3 diagenesis affects both the red and white dunes. The eogenic Type 3 diagenesis effectively "locked in" the reduced-porosity contact zone at an early stage, isolating the detrital red sediments from later large fluid fluxes. The oxidation and coating of the sand grains with hematite before deposition is supported by our observations of present-day migrating red dunes in the Namib desert and by numerous other examples cited (e.g, Folk 1976 and references therein).

Secondly, considering that both the red and white isolated dunes were deposited as red-hematite-coated eolian sands, the white isolated dunes must result from chemical bleaching. It is proposed that this bleaching may have resulted from reaction of grain-coating hematite with H_2S in hydrothermal groundwater, which has circulated through white dunes only. Hematite is reduced to form soluble ferrous iron that is transported away in solution (Fe_2O_3 depletion, Fig. 13B):

$$4\ Fe_2O_{3\,(s)} + H_2S_{\,(aq)} + 14\ H^+_{\,(aq)} \leftrightarrow 8\ Fe^{2+}_{\,(aq)} + SO_4^{2-}{}_{(aq)} + 8\ H_2O \qquad (1)$$

hematite + hydrogen sulfide + hydrogen (acid) ↔ iron + sulfate + water

This reaction should produce pyrite as noted by Kirkland et al. (1995), which has not been directly identified in the isolated white dunes. Pyrite is however present in the basalt and occasional hematite nodules are present in the white sandstone. These hematite nodules may be the later oxidation product of diagenetic pyrite. If no pyrite was present in the white sandstone it could suggest either (A) that the Fe^{2+} and SO_4^{2-} were able to migrate into the basalt before to precipitating or (B) that any H_2S in the aquifer rapidly reacted with the iron-rich basalt before to reducing iron in the red dunes. If the latter is true, the above reaction (1) was doubtfully in operation in the white dunes. An alternative explanation that requires less acid and no sulfur is that of a hydrothermal system with abundant dissolved hydrogen. Hydrogen could have been sourced from hot hydrothermal water interacting

with basalt (Stevens and McKinley 2000) or from magma degassing at depth (Arnórsson 1986). Hydrogen and carbon dioxide could then bleach the sandstone:

$$Fe_2O_{3\,(s)} + H_{2\,(aq)} + 2\,CO_{2\,(aq)} \leftrightarrow 2\,FeCO_{3\,(aq)} + H_2O_{\,(l)} \qquad (2)$$

hematite + hydrogen + carbon dioxide ↔ iron carbonate + water

The ferrous-iron carbonate would have then been transported away in solution (e.g, King, 1998).

Thirdly, the feldspar dissolution and mineral authigenesis observed in the sandstones in the study area is inferred to result from CO_2-rich hydrothermal fluids. White dunes are almost completely devoid of plagioclase feldspar (XRD analysis) and show reduced-strength orthoclase XRD peaks compared to red sandstone. Authigenic kaolinite, böhmite, and calcite, found in the white sandstone (Type 2), are not found in the red sandstone (Type 1) and are suggested to have formed at the expense of the feldspars during reaction with CO_2. Hangx and Spiers (2009) proposed and tested reactions between plagioclase feldspars and CO_2-H_2O under laboratory conditions simulating hydrothermal conditions. Both albite and anorthite were reacted under a variety of pressure and temperature conditions (200– 300 °C and 6– 18 MPa) with the aim to test the ideal reactions:

$$CaAl_2Si_2O_{8\,(s)} + CO_{2\,(aq)} + 2\,H_2O_{\,(l)} \leftrightarrow CaCO_{3\;\,(s)} + Al_2Si_2O_5(OH)_{4\,(s)} \qquad (3)$$

anorthite + carbon dioxide + water ↔ calcite + kaolinite

and

$$(K, Na)\,AlSi_3O_{8\,(s)} + CO_{2\,(aq)} + H_2O_{\,(l)} \leftrightarrow NaAlCO_3(OH)_{2\,(s)} + 3\,SiO_{2\,(s)} \qquad (4)$$

albite + carbon dioxide + water ↔ dawsonite + silica

Hangx and Spiers' (2009) results failed to fully replicate the above reactions and instead produced clays (kaolinite and smectite or illite), böhmite and a nickel, iron-hydrotalcite phase derived from their reaction vessel. Dawsonite and calcite were not produced in Hanx and Spiers' (2009) experiments, possibly due to subcritical solution state for crystal nucleation and conditions not being alkaline enough for dawsonite precipitation. Given sufficient time for further dissolution of plagioclase, carbonate phases would be anticipated (Hangx and Spiers 2009). It is proposed that in the white sandstone the Type 2 diagenesis is a natural analogue for the reactions observed by Hangx and Spiers (2009) based on the identical mineral reaction being observed. Calcite in the natural Type 2 white dunes is inferred to be the result of trace amounts of pre-existing carbonate

dust (common in eolian environments – Maurice Tucker, personal communication), and easily sourced locally by the erosion of carbonate-rich Precambrian basement rocks in the region. This dust provides the nuclei for calcite precipitation noted to be absent in Hanx and Spiers' (2009) experiments, as well as additional calcium and carbonate. The basalt-plagioclase-CO_2 reaction between the lava flows and sediments in our natural geological system produced enough Ca^{2+} ions for the additional calcite cementation to take place. This supports the proposed origin of the diagenetic fluids and suggests timing coincident with emplacement and cooling of the igneous intrusions in the area. Reaction of feldspar to form böhmite and kaolinite was also performed by Fu et al. (2009) on perthitic alkali feldspars under acidic hydrothermal conditions. Fu et al. (2009) noted the albite (Na- feldspar) component reacted preferentially, which conforms to the observation in Figure 12 and supports the Na depletion observed in sample NG29 (Fig. 13). The reactions between CO_2 and plagioclase provide an important natural analogue to processes under investigation relevant to industrial CO_2 sequestration (e.g, Matter et al. 2007; Matter and Kelemen 2009; Matter et al. 2016) and demonstrate how natural releases of CO_2 from igneous activity in sedimentary basins can be naturally moderated (e.g, Jones et al. 2016).

CONTROLS ON FLUID FLOW

Inasmuch as Type 2 diagenesis is a result of fluid flux and Type 1 diagenesis is a result of absence of this flux, it is logical to conclude that the enveloping lithology (lava) is responsible for compartmentalizing either individual dunes or volumes of rock encompassing dunes. If we consider that the lava is completely impermeable (which is unrealistic), it would also be logical to infer that fracture connectivity (i.e, faults and joints) controls fluid flow and some dunes are simply part of this fracture network and others have not been intersected. However, lava piles are not impermeable (e.g, Saar and Manga 1999); indeed, they can be major conductors of subsurface fluids, such as in the Columbia River Basalts, where the major aquifers are basalt (Newcomb 1961; see also Saar and Manga 1999), as well as in thick basaltic sequences offshore where high permeability can be preserved within flow tops (e.g, Millett et al. 2016). Permeability in pahoehoe lava flows is generally highest within the highly vesicular upper and lower crusts; the massive central lava cores show typically low permeability to nearly impermeable layers (Newcomb 1961; Smith 2004), where any permeability is restricted to cooling fractures (e.g, Petford 2003) or on the grain scale through alteration. A lava sequence can therefore be considered as having the potential to show markedly different porosity/permeability, with higher permeability layers running along lava flow tops (e.g, Millett et al., 2016).

584 The lowermost Tafelkop-type lava flows exhibit a compound-braided facies nature and do not form thick tabular
585 sheets (Jerram 2002). Such lava flows have markedly higher crust-to core-ratios (e.g, Nelson et al. 2009) and
586 contain abundant vesicles and fractures. The compound nature of these Tafelkop-type lavas in Dune Valley,
587 combined with the visible occurrence of highly vesicular zones, suggests that the lava was, at least partially
588 permeable in the horizontal direction. The stacking of many compound pahoehoe lava flows with relatively
589 permeable crusts and relatively impermeable cores would have resulted in a complex permeable network,
590 incapable of isolating dunes from fluid flow alone. Another element must be responsible for the
591 compartmentalization; we propose this to be the igneous dikes in the area. This hypothesis is supported by field
592 relationships in Dune C (Figs. 3, 16) where the dune is crosscut by an ~ 4 m-thick dolerite dike. An
593 impermeable contact zone is developed where the dike intersects the sandstone (similar to the hot type 3
594 diagenesis). The dike separates red Type 1 sand from white Type 2 sand. The dike follows the same ~ N-S trend
595 as most dikes in the Huab Outliers. Some dikes pass into and feed the lower Tafelkop lava (e.g, Jerram et al.
596 1999a) while others fed lavas that were younger than the youngest exposed lavas in the region, and can be seen
597 cutting up through the whole preserved sequence. Although it is possible that dike pathways are weaknesses that
598 can be reused by later phases of dike intrusion, the information from the dikes in the Huab Outliers suggests that
599 the timing and depth of compartment formation (igneous intrusion) could be from as little as 300 m of burial
600 (e.g, the feeder dikes) up to the complete thickness of the volcanic pile.

601 Fractures are irregular and poorly expressed in the Tafelkop basalt lavas due to the intense desert weathering,
602 but fractures would have formed during cooling and possibly subsequent tectonic activity. The presence of open
603 fractures and fissures is indirectly preserved due to sand infill (e.g, Jerram et al., 2000a; Jerram and Stollhofen
604 2002), creating molds of the fracture cavities. N-S-trending low-displacement faults (centimeters) frequently
605 cross cut sandstone beds in Dune Valley (Fig. 16), but they have not been found separating Type 1 sand from
606 Type 2 sand. Faults are frequently mineralized with calcite (also isotopically Type 2 affinity), and, depending on
607 timing, may have been pathways for the flow of diagenetic fluids. The relative timings of the diagenetic types is
608 presented in Figure 17, which highlights that Type 3 is restricted to lava flow (and in some cases dike
609 emplacement) during the volcanism, as these are “hot” contacts of the sand with the lava. The Type 1 and 2
610 diagenesis occurring largely during the later stages of synvolcanic burial and further burial of the sequence (Fig.
611 17).

612 A conceptual model of fluid flow in the basalt pile is given in Figure 18, to help explain the distribution and
613 compartmentalization of the Type 2 diagenesis. It is proposed that in the Tafelkop lavas, vertical to subvertical
614 igneous intrusions are largely responsible for isolating red dunes from diagenetic fluids (Fig. 18). The use of the
615 Type 2 sandstone as a tracer of fluid flow compartmentalized in a mixed basalt-siliciclastic system has identified
616 igneous dikes as the compartment-forming component, not the lava flows. This in part confirms the notion that
617 the dike system is acting as both a barrier laterally and modifying the permeability pathways of fluid flow (e.g,
618 Schofield et al., 2015; Senger et al., 2017). The exploitation of similar mixed-lithology hydrocarbon plays in
619 volcanic margins should consider the possible hydraulic connectivity of compound lava flows and sandstones
620 (e.g, the Faroe-Shetland basin and offshore Namibia), and be prepared to encounter dike-compartmentalized
621 reservoirs affecting charge and migration as well as the field development design required.

622 **IMPLICATIONS AND CONCLUSIONS**

623 1. Hot contacts at the bases of newly emplaced lava flows show a marked reduction in porosity and
624 permeability (Table 1, Fig. 9), as a result of rapid mechanical compaction of unconsolidated sand,
625 dissolution associated with hydrothermal activity generated by the degassing hot lava above, and
626 associated cementation. This “indurated” zone occurs a few tens of centimeters below these contacts,
627 resulting in the Type 3 diagenesis (Fig. 17).
628 2. Later fluid flow traced through inter-basalt sediments has been found to be heterogeneous and
629 controlled by igneous dike intrusions (e.g, Figs. 16, 18), some isolated sediment bodies being
630 connected to the flow regime, and some apparently isolated. The implication is that any fluid could be
631 controlled in this manner, including hydrocarbons. In the case in question, the Type 2 diagenesis
632 affected approximately half of the dunes exposed in Dune Valley, though the precise volume of
633 sandstone affected is not known.
634 3. These findings suggest that volume estimates of sediment-lava interbeded reservoirs (for petroleum
635 exploration), where encountered in the subsurface, should take into account that not all sediment bodies
636 predicted in similar situations will be charged with hydrocarbons, despite sharing stratigraphical
637 location, depositional environment and geological structure.
638 4. The Dune Valley outcrops of white sandstone have been identified as a natural analogue to the
639 proposed carbon sequestration method of Hangx and Spiers (2009); in our case magmatic CO_2 is being
640 sequestered. Our findings have implications for the total amount of CO_2 thought to have been emitted

641 from large igneous provinces (e.g, The Paraná-Etendeka or the Deccan Traps). Such estimates should
642 account for CO_2 that is sequestrated within sediments in hydraulic connection with the igneous
643 province (e.g, Caldeira and Ramoino 1990; Wignall 2001; McHone 2003; Jones et al. 2016) as well as
644 within the igneous rock themselves (Matter et al. 2016).
645 5. Apart from the tracing of heterogeneous hydrothermal fluid flow through the basalt pile, the results of
646 Type 2 diagenesis left reduced porosity and permeability compartments (the white sandstone), which
647 do not relate to depositional environment or geological structure. These poorer potential reservoir rocks
648 are connected to the fluid migration pathways, whereas the better-reservoir-quality red sandstones are
649 not (at least at the time of hydrothermal activity). This dichotomy should be appreciated if similar rocks
650 are encountered during exploration in volcanic provinces. For instance, development of mixed basalt-
651 siliciclastic reservoirs (such as Rosebank) should not expect all stratigraphically trapped sandstone
652 units in the play to show identical diagenesis, and hence reservoir properties. Conversely, if exploration
653 drilling encounters poor-quality sandstone, with evidence of Type 2 diagenesis, it should be considered
654 that good-quality sandstone may exist in close proximity.

655 **ACKNOWLEDGMENTS**

656 We would like to thank the VMRC partners (Chevron, ENI, DONG, Statoil, OMV and HESS) and
657 OneNortheast (sponsored by Rick Smith, FWS Consultants) for funding this project. This work was also partly
658 supported by the Research Council of Norway through its Centers of Excellence funding scheme, project
659 number 223272 (CEED). We would like to thank Joanna Garland of Cambridge Carbonates Ltd. who provided
660 valuable feedback during the final preparation of the manuscript. We thank Andrew Hurst and Colin Taylor
661 (Aberdeen) and Nicholas Odling (Edinburgh) for facilitating laboratory work. Breno Waichel (and Brazilian
662 colleagues), Tim Watton, Sam Clark, Alex Baker, Kevin Purvis and Victoria Gee are thanked for help and
663 guidance. Gabi Schneider and the staff at the Geological Survey of Namibia are thanked for their continued
664 support in Namibia. We thank Sally Sutton, Nick Schofield, and an anonymous reviewer for thoughtful
665 comments. Leslie Melim is thanked for editorial guidance and John Southard is thanked for detailed technical
666 edits; they have significantly improved the manuscript, especially regarding organization.

667 **REFERENCES**

668 Arnórsson, S., 1986, Chemistry of gases associated with geothermal activity and volcanism in Iceland: A
669 review: Journal of Geophysical Research: Solid Earth, v. 91, p. 12261-12268.

Angkasa, S.S., Jerram, D.A., Millett, J.M., Svensen, H.H., Planke, S., Taylor, R.A., Schofield, N. and Howell, J., 2017, Mafic intrusions, hydrothermal venting, and the basalt-sediment transition: Linking onshore and offshore examples from the North Atlantic igneous province: Interpretation, v.5(3), SK83-SK101.

Beitler, B., Chan, M., and Parry, W., 2003, Bleaching of Jurassic Navajo sandstone on Colorado Plateau Laramide highs: Evidence of exhumed hydrocarbon supergiants?: Geology, v. 31, p. 1041-1044.

Beitler, B., Parry, W., and Chan, M., 2005, Fingerprints of fluid flow: chemical diagenetic history of the Jurassic Navajo Sandstone, southern Utah, USA: Journal of Sedimentary Research, v. 75, p. 547-561.

Beswetherick, S., Miglio, G., Ross, A., and Poynter, S., 2009, The Ann-Marie Prospect, Licence 005. Faroe Islands Exploration Conference: Proceedings of the 2nd Conference. Annales Societatis Scientiarum Færoensis, Supplementum, v. 50, p. 246-266.

Bowen, G.J., and Wilkinson, B., 2002, Spatial distribution of $\delta^{18}O$ in meteoric precipitation: Geology, v. 30, p. 315-318.

Brownlow, A.H., 1996, Geochemistry: Upper Saddle River, New Jersey, Prentice Hall, 580 p.

Bryan, S.E., Ukstins Peate, I., Peate, D.W., Self, S., Jerram, D.A., Mawby, M.R., Marsh, J.S., and Miller, J.A., 2010, The largest volcanic eruptions on Earth: Earth-Science Reviews, v. 102(3), p. 207-229.

Cai, W., Yu, J., Cheng, B., Su, B.L., and Jaroniec, M., 2009, Synthesis of boehmite hollow core/shell and hollow microspheres via sodium tartrate-mediated phase transformation and their enhanced adsorption performance in water treatment: Journal of Physical Chemistry *C*, v. 113, p. 14,739-14,746.

Caldeira, K., and Rampino, M.R., 1990, Carbon dioxide emissions from Deccan volcanism and a K/T boundary greenhouse effect: Geophysical Research Letters, v. 17, p. 1299-1302.

Candy, I., Adamson, K., Gallant, C.E., Whitfield, E., and Pope, R, 2012, Oxygen and carbon isotopic composition of Quaternary meteoric carbonates from western and southern Europe: Their role in palaeoenvironmental reconstruction: Palaeogeography, Palaeoclimatology, Palaeoecology, v. 326-328, p. 1-11.

Chan, M.A., Parry, W.T., and Bowman, J.R, 2000, Diagenetic hematite and manganese oxides and fault-related fluid flow in Jurassic sandstones, Southeastern Utah: AAPG, Bulletin, v. 84, p. 1281-1310.

Clemson, J., Cartwright, J., and Booth, J., 1997, Structural segmentation and the influence of basement structure on the Namibian passive margin: Geological Society of London, Journal, v. 154, p. 477-482.

Davison, I., 1999, Tectonics and hydrocarbon distribution along the Brazilian South Atlantic margin, *in* Cameron, N.R., Bate, R.H., and Clure, V.S., eds., The oil and gas habitats of the South Atlantic: Geological Society, London, Special Publication, v. 153, p. 133-151.

700 Delmelle, P., and Stix., 2000, Volcanic gases, *in* Sigurdsson, H. et al., eds., Encyclopaedia of Volcanoes:
701 Academic press, p. 803-145.
702 Dias, Á.S., Früh-Green, G. L., Bernasconi, S. M., and Barriga, F.J.A.S, 2011, Geochemistry and stable isotope
703 constraints on high-temperature activity from sediment cores of the Saldanha hydrothermal field: Marine
704 Geology, v. 279, p. 128-140.
705 Dickinson, W., and Milliken, K., 1995, The diagenetic role of brittle deformation in compaction and pressure
706 solution, Etjo sandstone, Namibia: The Journal of Geology, v. 103, p. 339-347.
707 Dodd. S.C., Niocaill, C.M., and Muxworthy, A.R., 2015, Long duration (>4 Ma) and steady-state volcanic
708 activity in the early Cretaceous Paraná–Etendeka Large Igneous Province: New palaeomagnetic data from
709 Namibia: Earth and Planetary Science Letters, v. 414, p. 16-29.
710 Duncan, A.R., Newton, S.R., van den Berg, C., and Reid, D.L., 1989, Geochemistry and petrology of dolerite
711 sills in the Huab River Valley, Damaraland, north-western Namibia: Geological Survey of Namibia,
712 Communications, v. 5, p. 5-18.
713 Folk, R.L., 1976, Reddening of desert sands: Simpson Desert, NT, Australia: Journal of Sedimentary Petrology,
714 v. 46, p. 604-615.
715 França, A., Araújo, L., Maynard, J., and Potter, P., 2003, Secondary porosity formed by deep meteoric leaching:
716 Botucatu eolianite, southern South America: AAPG, bulletin, v. 87, p. 1073-1082.
717 Fu, Q., Lu, P., Konishi, H., Dilmore, R., Xu, H., Seyfried, W.E. Jr., and Zhu, C., 2009, Coupled alkali-feldspar
718 dissolution and secondary mineral precipitation in batch systems: 1. New experiments at 200 °C and 300 bars:
719 Chemical Geology, v. 258, p. 125-135.
720 Garden, I.R., Guscott, S.C., Burley, S.D., Foxford, K.A., Walsh, J.J., and Marshall, J, 2001, An exhumed
721 palaeo-hydrocarbon migration fairway in a faulted carrier system, Entrada Sandstone of SE Utah, USA:
722 Geofluids, v. 1, p. 195-213.
723 Gierlowski-Kordesch, E.H., Weismiller, H.C., Stigall, A.L., and Hembree, D.I., 2015, Pedogenic mud
724 aggregates and sedimentation patterns between basalt flows (Jurassic Kalkrand Formation, Namibia), *in* Larsen,
725 D., Egenhoff, S.O., and Fishman, N.S., eds., Paying Attention to Mudrocks: Priceless!: Geological Society
726 of America Special Paper 515, p. 65–86.
727 Gilg, H.A., Morteani, G., Kostitsyn, Y., Preinfalk, C., Gatter, I., and Strieder, A.J, 2003, Genesis of amythyst
728 geodes in basaltic rocs of the Serra Geral Formation (Ametista do Sul, Rio Grande do Sul, Brazil): a fluid

729 inclusion, REE, oxygen, carbon, and Sr study on basalt, quartz and calcite: Mineralium Deposita, v. 38, p. 1009-
730 1025.
731 Goudie, A.S., and Eckardt, F., 1999, The evolution of the morphological framework of the central Namib
732 Desert, Namibia, since the Early Cretaceous: Geografiska Annaler, Series A, Physical Geography, p. 81, v. 443-
733 458.
734 Grove, C., and Jerram, D.A., 2011, jPOR: An ImageJ macro to quantify total optical porosity from blue-stained
735 thin sections: Computers & Geosciences, v. 37, p. 1850-1859.
736 Hangx, S.J.T., and Spiers, C.J., 2009, Reaction of plagioclase feldspars with CO_2 under hydrothermal
737 conditions: Chemical Geology, v. 265, p. 88-98.
738 Hazewinkel, M., ed., 2001, "Student test": Encyclopedia of Mathematics, Springer, ISBN 978-1-55608-010-4
739 Helland-Hansen, D., 2009, Rosebank – Challenges to development from a subsurface perspective: Faroe Islands
740 Exploration Conference: Proceedings of the 2nd Conference: Annales Societatis Scientiarum Færoensis,
741 Supplementum, v. 50, p. 241-245.
742 Henley, R.W., and Ellis, A.J., 1983, Geothermal systems ancient and modern: a geochemical review: Earth-
743 Science Reviews, v. 19, p. 1-50.
744 Hitchen, K., Johnson, H., and Gatliff, R.W., eds., 2013, Geology of the Rockall Basin and Adjacent Areas:
745 British Geological Survey, Keyworth, Nottingham, UK, 193 p.
746 Horsthemke, E., Ledendeker, S., and Porada, H., 1990, Depositional environments and stratigraphic correlation
747 of the Karoo Sequence in northwestern Damaraland: Geological Survey of Namibia, Communications, v. 6, p.
748 63-73.
749 Horton, T.W., Atkinson, L., and Oze, C, 2012, Hydrothermal carbonate geochemistry of the Ngatamariki
750 subsurface reservoir, New Zealand: Proceedings of the Thirty-Seventh Workshop on Geothermal Reservoir
751 Engineering, Stanford, California, p. 1-8.
752 Howell, J., and Mountney, N., 2001, Aeolian grain flow architecture: hard data for reservoir models and
753 implications for red bed sequence stratigraphy: Petroleum Geoscience, v. 7, p. 51-56.
754 Hurst, A., and Goggin, D., 1995, Probe permeametry: An overview and bibliography: AAPG, bulletin, v. 79, p.
755 463-463.
756 Jerram, D.A., Mountney, N., Holzförster, F., and Stollhofen, H., 1999a, Internal stratigraphic relationships in the
757 Etendeka Group in the Huab Basin, NW Namibia: understanding the onset of flood volcanism: Journal of
758 Geodynamics, v. 28, p. 393-418.

759 Jerram, D.A., Mountney, N., and Stollhofen, H., 1999b, Facies architecture of the Etjo Sandstone Formation and
760 its interaction with the Basal Etendeka Flood Basalts of northwest Namibia: implications for offshore
761 prospectivity *in* Cameron, N.R., Bate, R.H., and Clure, V.S., eds., The oil and gas habitats of the South Atlantic
762 Geological Society, London, Special Publication, v. 153, p. 367-380.
763 Jerram, D.A., Mountney, N., Howell, J., Long, D., and Stollhofen, H., 2000a, Death of a sand sea: an active
764 aeolian erg systematically buried by the Etendeka flood basalts of NW Namibia: Geological Society of London,
765 Journal, v. 157, p. 513-516.
766 Jerram, D.A., Mountney, N., Howell, J., and Stollhofen, H., 2000b, The Fossilised Desert: recent developments
767 in our understanding of the Lower Cretaceous deposits in the Huab Basin, NW Namibia: Geological Survey of
768 Namibia, Communications, v. 12, p. 269-278.
769 Jerram, D.A., and Robbe, O., 2001, Building a 3-D geologic model of a flood basalt: an example from the
770 Etendeka, NW Namibia: Visual Geosciences, v. 6, p.1-8.
771 Jerram, D.A., 2002, Volcanology and faces architecture of flood basalts: Volcanic Rifted Margins, v. 362, p.
772 119.
773 Jerram, D.A., and Stollhofen, H., 2002, Lava–sediment interaction in desert settings: are all peperite-like
774 textures the result of magma–water interaction?: Journal of Volcanology and Geothermal Research, v. 114, p.
775 231-249.
776 Jerram, D.A., and Widdowson, M., 2005, The anatomy of Continental Flood Basalt Provinces: geological
777 constraints on the processes and products of flood volcanism: Lithos, v. 79, p. 385-405.
778 Jones, M.T., Jerram, D.A., Svensen, H., and Grove, C., 2016, The effects of large igneous provinces on the
779 global carbon and sulphur cycles: Palaeogeography, Palaeoclimatology, Palaeoecology, v. 441, p. 4-21.
780 Jungslager, E.H.A., 1999, Petroleum habitats of the Atlantic margin of South Africa prospectivity *in* Cameron,
781 N.R., Bate, R.H., and Clure, V.S., eds., The oil and gas habitats of the South Atlantic Geological Society,
782 London, Special Publication, v. 153 p. 153-168.
783 King, D.W., 1998, Role of carbonate speciation on the oxidation rate of Fe(II) in aquatic systems:
784 Environmental Science & Technology, v. 32, p. 2997-3003.
785 Kirkland, D.W., Denison, R.E., and Rooney, M.A., 1995, Diagenetic alteration of Permian strata at oil fields of
786 south central Oklahoma, USA: Marine and Petroleum Geology, v. 12, p. 629-644.
787 Lowenstern, J., 2001, Carbon dioxide in magmas and implications for hydrothermal systems: Mineralium
788 Deposita, v. 36, p. 490-502.

789 Lundegard, P.D., 1992, Sandstone porosity loss: a" big picture" view of the importance of compaction: Journal
790 of Sedimentary Petrology, v. 62, p. 250-260.
791 Ma, Y., Liu, C., Zhao, J., Huang, L., Yu, L., and Wang, J., 2007, Characteristics of bleaching of sandstone in
792 northeast of Ordos Basin and its relationship with natural gas leakage: Science in China Series D: Earth
793 Sciences, v. 50, p. 153-164.
794 Matter, J.M., Takahashi, T., and Goldberg, D., 2007, Experimental evaluation of in situ CO_2-water-rock
795 reactions during CO_2 injection in basaltic rocks: Implications for geological CO_2 sequestration: Geochemistry,
796 Geophysics, Geosystems, v. 8, No. 2.
797 Matter, J.M., and Kelemen, P.B., 2009, Permanent storage of carbon dioxide in geological reservoirs by mineral
798 carbonation: Nature Geoscience, v. 2, p. 837-841.
799 Matter, J.M., Stute, M., Snæbjörnsdottir, S.Ó., Oelkers, E.H., Gislason, S.R., Aradottir, E.S., Sigfusson, B.,
800 Gunnarsson, I., Sigurdardottir, H., Gunnlaugsson, E., and Axelsson, G., 2016, Rapid carbon mineralization for
801 permanent disposal of anthropogenic carbon dioxide emissions: Science, v. 352(6291), p. 1312-1314.
802 Marsh, J.S., Erlank, A.J., and Duncan, A.R., 1991, Preliminary geochemical data for dolerite dykes and sills of
803 the southern part of the Etendeka Igneous Province: Geological Survey of Namibia, Communications, v. 7, p.
804 71-74.
805 Marsh, J.S., Ewart, A., Milner, S., Duncan, A., and Miller, R., 2001, The Etendeka Igneous Province: magma
806 types and their stratigraphic distribution with implications for the evolution of the Parana-Etendeka flood basalt
807 province: Bulletin of Volcanology, v. 62, p. 464-486.
808 Marx, V.L., 2009, Impacts of upstream uses on the alluvial aquifer of the Swakop River, Namibia
809 [Diplomarbeit]: Albert Ludwig Universität Freiburg, Germany, 85 p.
810 McHone, J.G., 2003, Volatile emissions from central Atlantic magmatic province basalts: mass assumptions and
811 environmental consequences: American Geophysical Union, Geophysical Monograph, v. 136, p. 241-254.
812 McLachlan, I.R., 1990, Introductory note on the history of the Kudu prospect: Geological Survey of Namibia,
813 Communications, v. 6, p. 5.
814 Millett, J.M., Wilkins, A.D., Campbell, E., Hole, M.J., Taylor, R.A., Healy, D., Jerram, D.A., Jolley, D.W.,
815 Planke, S., Archer, S.G. and Blischke, A., 2016, The geology of offshore drilling through basalt sequences:
816 Understanding operational complications to improve efficiency: Marine and Petroleum Geology, v. 77, p. 1177-
817 1192.

818 Milner, S., Duncan, A., Whittingham, A., and Ewart, A., 1995, Trans-Atlantic correlation of eruptive sequences
819 and individual silicic volcanic units within the Paraná-Etendeka igneous province: Journal of Volcanology and
820 Geothermal Research, v. 69, p. 137-157.
821 Moulton, G.F., 1926, Some features of redbed bleaching: AAPG, bulletin, v. 10, p. 304-311.
822 Mountney, N., Howell, J., Flint, S., and Jerram, D., 1998, Aeolian and alluvial deposition within the Mesozoic
823 Etjo Sandstone Formation, northwest Namibia: Journal of African Earth Sciences, v. 27, p. 175-192.
824 Mountney, N., Howell, J., Flint, S., and Jerram, D., 1999a, Relating eolian bounding-surface geometries to the
825 bed forms that generated them: Etjo Formation, Cretaceous, Namibia: Geology, v. 27, p. 159.
826 Mountney, N., Howell, J., Flint, S., and Jerram, D., 1999b, Climate, sediment supply and tectonics as controls
827 on the deposition and preservation of the aeolian-fluvial Etjo Sandstone Formation, Namibia: Geological
828 Society of London, Journal, v. 156, p. 771-777.
829 Naylor, H., Turner, P., Vaughan, D.J., and Fallick, A.E, 1989, The Cherty Rock: a petrographic and isotopic
830 study of a Permo Triassic calcrete: Geological Journal, v. 24, p. 205-221.
831 Nelson, C., Jerram, D., and Hobbs, R., 2009, Flood basalt facies from borehole data: implications for
832 prospectivity and volcanology in volcanic rifted margins: Petroleum Geoscience, v. 15, p. 313-324.
833 Newcomb, R.C., 1961, Storage of ground water behind subsurface dams in the Columbia River Basalt,
834 Washington, Oregon, and Idaho: Geological Survey Professional Paper, 383-A, Washington, US Government
835 Printing Office.
836 O'Neil, J.R., Clayton, R.N., and Mayeda, T.K., 1969, Oxygen isotope fractionation in divalent metal carbonates:
837 Journal of Chemical Physics, v. 51, p. 5547-5558.
838 Parry, W., Chan, M., and Beitler, B., 2004, Chemical bleaching indicates episodes of fluid flow in deformation
839 bands in sandstone: AAPG, bulletin, v. 88, p. 175-191.
840 Peate, D., 1997, The Paraná-Etendeka Province: American Geophysical Union, Geophysical Monograph, v.
841 100, p. 217-246.
842 Peate, I.U., Larsen, M., and Lesher, C.E., 2003, The transition from sedimentation to flood volcanism in the
843 Kangerlussuaq Basin, East Greenland: basaltic pyroclastic volcanism during initial Palaeogene continental
844 break-up: Geological Society of London, Journal, v. 160, p. 759-772.
845 Petford, N., 2003, Controls on primary porosity and permeability development in igneous rocks *in* Petford, N.,
846 and McCaffrey, K.J.W., eds., Hydrocarbons in Crystalline Rocks: Geological Society of London, Special
847 Publication, v. 214, p. 93-107.

848 Petry, K., Jerram, D.A., del Pilar M, de Almeida, D., and Zerfass, H., 2007, Volcanic-sedimentary features in
849 the Serra Geral Fm. Paraná Basin, southern Brazil: examples of dynamic lava-sediment interactions in an arid
850 setting: Journal of Volcanology and Geothermal Research, v. 159, p. 313-325.
851 Platt, J.D., 1994, Geochemical evolution of pore waters in the Rotliegend (Early Permian) of northern Germany:
852 Marine and Petroleum Geology, v. 11, p. 66-78.
853 Purvis, K., and Wright, V.P, 1991, Calcretes related to phreatophytic vegetation from the Middle Triassic Otter
854 Sandstone of South West England: Sedimentology, v. 88, p. 539-551.
855 Raab, M., Brown, R., Gallagher, K., Weber, K., and Gleadow, A., 2005, Denudational and thermal history of the
856 Early Cretaceous Brandberg and Okenyenya igneous complexes on Namibia's Atlantic passive margin:
857 Tectonics, v. 24, No. 3.
858 Rateau, R., Schofield, N., and Smith, M., 2013, The potential role of igneous intrusions on hydrocarbon
859 migration, West of Shetland: Petroleum Geoscience, v. 19, p. 259-272.
860 Rollinson, H.R., 1993, Using Geochemical Data; Evaluation, Eresentation, Interpretation: Harlow, Pearson
861 Education, 352 p.
862 Ross, P.S., Ukstins Peate, I., McClintock, M., Xu, Y., Skilling, I., White, J., and Houghton, B., 2005, Mafic
863 volcaniclastic deposits in flood basalt provinces: a review: Journal of volcanology and Geothermal Research, v.
864 145, p. 281-314.
865 Rye, R.O., 2005, A review of the stable-isotope geochemistry of sulfate minerals in selected igneous
866 environments and related hydrothermal systems: Chemical Geology, v. 215, p. 5-36.
867 Saar, M., and Manga, M., 1999, Permeability-porosity relationship in vesicular basalts: Geophysical Research
868 Letters, v. 26, p. 111-114.
869 Schofield, N., and Jolley, D.W., 2013, Development of intra-basaltic lava-field drainage systems within the
870 Faroe-Shetland Basin: Petroleum Geoscience. v. 19, p. 273-288.
871 Schofield, N., Holford, S., Millett, J., Brown, D., Jolley, D., Passey, S.R., Muirhead, D., Grove, C., Magee, C.,
872 Murray, J., Hole, M., Jackson, C.A.-L., and Stevenson, C., 2015, Regional magma plumbing and emplacement
873 mechanisms of the Faroe-Shetland Sill Complex: implications for magma transport and petroleum systems
874 within sedimentary basins: Basin Research, v. 29, p. 41-63.
875 Schreiber, U.M., 2006, Geological Map of Namibia 1: 250 000 Geological Series, Sheet 2014 – Fransfontein
876 (Provisional): Geological Survey of Namibia.

877 Scherer, C., 2002, Preservation of aeolian genetic units by lava flows in the Lower Cretaceous of the Paraná
878 Basin, southern Brazil: Sedimentology, v. 49, p. 97-116.
879 Scherer, C.M.S., and Goldberg, K., 2007, Palaeowind patterns during the latest Jurassic- earliest Cretaceous in
880 Gondwana: evidence from aeolian cross strata of the Botucatu Formation, Brazil: Palaeogeography,
881 Palaeoclimatology, Palaeoecology, v. 248, p. 1-10.
882 Schöner, R., and Gaupp, R., 2005, Contrasting red bed diagenesis: the southern and northern margin of the
883 Central European Basin: International Journal of Earth Sciences, v. 94, p. 897-916.
884 Schutter, S.R., 2003, Hydrocarbon occurrence and exploration in and around igneous rocks *in* Petford, N., and
885 McCaffrey, K.J.W., eds., Hydrocarbons in Crystalline Rocks: Geological Society of London, Special
886 Publication, v. 214, p. 7-33.
887 Scotese, C.R., 2001, Atlas of Earth History, Volume 1, Palaeogeography: PALEOMAP Project, Arlington,
888 Texas, 52 p.
889 Self, S., Keszthelyi, L., and Thordarson, T., 1998, The importance of pahoehoe: Annual Review of Earth and
890 Planetary Sciences, v. 26, p. 81-110.
891 Senger, K., Millett, J., Planke, S., Ogata, K., Eide, C.H., Festøy, M., Galland, O., and Jerram, D.A., 2017,
892 Effects of igneous intrusions on the petroleum system: a review: First Break, v. 35, no. 6, p. 47-56.
893 Shevenell, L., and Goff, F., 1993, Addition of magmatic volatiles into the hot spring waters of Loowit Canyon,
894 Mount St. Helens, Washington, USA: Bulletin of Volcanology, v. 55, p. 489-503.
895 Simmons, S., and Christenson, B., 1994, Origins of calcite in a boiling geothermal system: American Journal of
896 Science, v. 294, p. 361-400.
897 Smallwood, J.R., Prescott, D., and Kirk, W., 2004, Alternatives in Paleocene exploration West of Shetland: a
898 case study: Scottish Journal of Geology, v. 40, p. 131-143.
899 Smith, R.P., 2004, Geologic setting of the Snake River Plain Aquifer and vadose zone: Vadose Zone Journal, v.
900 3, no. 1, p. 47-58.
901 Solomons, W., Goudie, A., and Mook, W.G., 1978, Isotopic composition of calcrete deposits from Europe,
902 Africa and India: Earth Surface Processes, v. 3, p. 43-57.
903 Stanistreet, I., and Stollhofen, H., 1999, Onshore equivalents of the main Kudu gas reservoir in Namibia *in*
904 Cameron, N.R., Bate, R.H., and Clure, V.S., eds., The oil and gas habitats of the South Atlantic: Geological
905 Society of London, Special Publication, v. 153, p. 345-365.

906 Stevens, T.O., and McKinley, J.P., 2000, Abiotic controls on H_2 production from basalt-water reactions and
907 implications for aquifer biogeochemistry: Environmental science & technology, v. 34, p. 826-831.
908 Surdam, R.C., Jiao, Z.S., and MacGowan, D.B., 1993, Redox reactions involving hydrocarbons and mineral
909 oxidants: A mechanism for significant porosity enhancement in sandstones: AAPG, bulletin, v. 77, p. 1509-
910 1518.
911 Waichel, B.L., Scherer, C., and Frank, H.T., 2008, Basaltic lava flows covering active aeolian dunes in the
912 Paraná Basin in southern Brazil: Features and emplacement aspects: Journal of Volcanology and Geothermal
913 Research, v. 171, p. 59-72.
914 Waichel, B.L., de Lima, E.F., Viana, A.R., Scherer, C.M., Bueno, G.V., and Dutra, G., 2011, Stratigraphy and
915 volcanic facies architecture of the Torres Syncline, Southern Brazil, and its role in understanding the Paraná-
916 Etendeka Continental Flood Basalt Province: Journal of Volcanology and Geothermal Research, v. 215, p. 74-
917 82.
918 Watton, T.J., Cannon, S., Brown, R.J., Jerram, D.A., and Waichel, B.L., 2014, Using formation micro-imaging,
919 wireline logs and onshore analogues to distinguish volcanic lithofacies in boreholes: examples from Palaeogene
920 successions in the Faroe-Shetland Basin, NE Atlantic *in* Cannon, SJC., and Ellis, D., eds., Hydrocarbon
921 Exploration to Exploitation West of Shetlands: Geological Society of London, Special Publication, v. 397, p.
922 173-192.
923 Walker, G.P.L., 1971, Compound and simple lava flows and flood basalts: Bulletin of Volcanology, v. 35, p.
924 579-590.
925 White, D., 1957, Thermal waters of volcanic origin: Geological Society of America, Bulletin, v. 68, p. 1637.
926 Wignall, P.B., 2001, Large igneous provinces and mass extinctions: Earth-Science Reviews, v. 53, p. 1-33.
927 Wu, X., Zhang, B., Wang, D., and Hu, Z., 2012, Morphology evolution studies of boehmite hollow
928 microspheres synthesized under hydrothermal conditions: Materials Letters, v. 70, p. 128-131.
929
930
931
932 Fig. 1. A) Location of Namibia in southern Africa. B) Distribution of Lower Cretaceous subaerial outcrop in
933 Namibia (sediments and lava flows). Sediments are predominantly the Twyfelfontein Formation sandstones and
934 lavas Paraná-Etendeka basalts, basaltic andesites, and silicic rheoignimbrites. Huab outliers in red box. C)
935 Cretaceous subaerial outcrop (sediments and lava flows) in the Huab Outliers. Dune valley in yellow box. Maps

936 compiled from own field mapping, Landsat 7 ETM+ imagery and maps published by the Geological Survey of
937 Namibia.

938

939 Fig. 2. Stratigraphic succession of the Huab Basin (adapted from Jerram et al. 1999a). The units of interest form
940 the upper parts of the Twyfelfontain Fm. and lower parts of the Awahab Fm. The relative distribution of
941 Etendeka-related intrusions is also given (Kdo, green column). Note that the Awahab and Twyfelfontain Fms.
942 are indicated as overlapping due to the interbedded nature of the sedimentary and igneous rocks.

943

944 Fig. 3. Geological map of Dune Valley. Barchnoid dunes detailed in this contribution are labelled (A, B, C).
945 Point P and Q = origin of photographs in Fig. 5. The isolated nature of barchanoid dunes in the basaltic lava
946 flows is evident from the map.

947

948 Fig. 4. Schematic diagram of passive drowning of Twyfelfontein erg system in the Huab Basin by Lower
949 Cretaceous Basalts (mainly Tafelkop type basalts in Huab Outliers south of Huab River and a mix of Tafelkop
950 and Tafelberg-type basalts along the main river sections). The transverse-draa-dominated major erg is first
951 drowned (A), which restricts sediment mobility. Remaining unburied sediment is reworked to form minor erg
952 (B) and bypass surfaces where sand infiltrates basalt cooling cracks but does not form dunes. The minor erg is
953 then drowned by lava. Further lava drowning isolates more sediment from the active eolian system creating a
954 sediment-poor eolian system of isolated barchanoid dunes (C), which are themselves drowned by lava.
955 Successive drowning locks up more sediment until no more dunes are formed on lava surfaces (D). This is
956 followed by differential diagenesis to form red and white sandstone. Drowning sequence is modified from
957 Jerram et al. (1999a, 2000).

958

959 Fig. 5. A) Photograph of Dune Valley taken from the top of Awahab/Mikberg mountain (facing ~ SSW),
960 numerous isolated dunes/sand bodies visible, completely preserved barchans dunes, Dune A (Type 3 white) and
961 Dune B (Type 2 red) are labelled. B) Close-up of completely preserved barchan dune, with inset showing
962 detailed measurements around the dune (adapted from Jerram et al. 2000a). C) Photograph of Dune B (facing

963 south from point Q Fig. 3), the contrasting sand color apparent together with equivalent stratigraphic level and
964 proximity to each other. See Fig. 2 for stratigraphic labels.

965

966 Fig. 6. Geological map of Dune Valley showing a higher resolution of Dune A white and Dune B red sampled in
967 this study. Contour spacing is 10 m, rock unit abbreviations are as in Fig. 2.

968 Table. 1. Average point-counting data for each "type" of diagenesis identified in this study. 500 points were
969 counted for each sample (See also Grove and Jerram 2011).

970 Table. 2. Petrological and mineralogical comparison of contact sediments at Dune A white and Dune B red.

971 Table. 3. T-Test results of the point counting and permeability analysis of Type 1 red dunes and Type 2 white
972 dunes (see table 2). All parameters other than opaque minerals have a T-Test result showing that the phase
973 counted is either statistically significantly different (95%) or highly statistically significantly different (99%).
974 The opaque-mineral result supports the hypothesis that iron oxides are reprecipitated locally as nodules. Highly
975 statistically significant results are appended with an asterisk.

976 Fig. 7. Photomicrographs of sandstone at basalt contact for both white (sample NG26) and red (NG31) dunes to
977 illustrate Type 3 diagenesis. A) NG26, white, shows increased compaction over the control, calcite cement,
978 hematite grain coatings, and relatively unaltered feldspars (cf. Fig. 8). B) NG31, red, shows increased
979 compaction over the control, calcite cement and hematite grain coatings. C) NG52, which is a control sample
980 from major erg not in close proximity to igneous rocks; cementation and compaction are less than both samples
981 at the contact with lava. No appreciable difference exists between Dune A (white) and Dune B (red) examples at
982 the hot contacts, with the original porosity being occluded predominantly by calcite. K = potassium feldspar, Il
983 = ilmenite, Calc = calcite, Haem = hematite.

984 Fig. 8. Photomicrographs of the white sandstone illustrating Type 2 diagenesis and comparing with red Type 1
985 diagenesis. A) NG33 Dune B red 2 m below hot contact, connected pores, both K-spar and plagioclase detrital
986 grains present. B, C) Dune A white 2 m below hot lava contact, kaolinite and calcite fills pores replacing
987 plagioclase and some k-spar, which has enabled increased compaction. D, E) Dune A white, 3 m below hot lava
988 contact, diagenetic assemblage is same as NG28, part E shows a plagioclase being transformed to kaolinite.

989 Thin sections stained for K-spar and carbonates. K = K-spar, calc = calcite, kao = kaolinite, q-og = quartz
990 overgrowth, Haem = hematite, PPL = plane polarized Light, XPL = cross polarized light.

991 Fig. 9. A) Graph of porosity against distance from contact for Dune A (white), Dune B (red), and other isolated
992 dunes in Dune Valley (white or red, see table 3). All porosities decrease toward hot contact, red dunes regain
993 porosity more rapidly due to absence of secondary hydrothermal alteration (Type 2 diagenesis). Linear trend
994 lines shown for Dune A white (blue) and Dune B red (red) both show good correlations with distance. B)
995 Compaction-porosity loss (COPL) and cementation-porosity loss (CEPL) against distance below lava for Dune
996 A (white), Dune B (red), and other isolated dunes in Dune Valley (white or red). COPL increases rapidly within
997 30 cm of contact due to loading of lava on unconsolidated sediment combined with effects of corrosive volcanic
998 gases on feldspar grains.

999 Fig. 10. A) Relationship between probe permeability (logarithmic scale) and distance below hot contact for red
1000 and white dunes. Both types of permeability decrease in proximity to the contact zone, but white dunes do not
1001 increase to equal levels of red dunes. Linear regression trends are shown for white Dune A (blue) and red Dune
1002 B (red). B) Relationship between porosity and permeability for red and white dunes. Note separation of red and
1003 white dunes.

1004 Fig. 11. SEM images of rock chips from Type 2 white sandstone. A) Authigenic assemblage of böhmite (bö),
1005 kaolinite (kao), and calcite (calc). B) Kaolinite is totally replacing feldspar grains, and böhmite is coating quartz
1006 and a relic feldspar in bottom right. C) Plagioclase being replaced by kaolinite and böhmite; this was the only
1007 identifiable plagioclase grain encountered in the study. D) Close-up of kaolinite and böhmite authigenic
1008 minerals. Q = quartz, plag = plagioclase, p = pore.

1009 Fig. 12. X-ray diffraction spectra for samples NG32 (red line, red sand, Type 1) and NG29 (blue line, white
1010 sand, Type 2); important peaks are labelled. Plagioclase (albite and anorthite) peaks present in red sand are
1011 absent in white sand, consistent with petrographical observations. White sand has peaks for kaolinite or chlorite
1012 but red sand does not. Orthoclase peaks are also weakened in white sand. Interestingly no peak for böhmite was
1013 produced despite its identification under SEM. kao= kaolinite, ch= chlorite, alb= albite, an= anorthite, or=
1014 orthoclase.

1015 Fig. 13. Graph of major-element data in Appendix 2 normalized to NG52 values. A) NG32 red dune (red line)
1016 and NG29 white dune (blue line). NG29 white has enriched CaO, and increased LOI. NG29 is leached of Na_2O

and Fe_2O_3. B) NG26 white contact (blue line) and NG31 red contact (red line). CaO is enriched in both contact samples, other elements except MnO show little variation, suggesting that both contacts (red and white dunes) are the same.

Fig. 14. Graphs for Dune A white, Dune B red, other white dunes, and other red dunes against distance below hot contact. A) Authigenic quartz shows little correlation with distance because it is formed during burial, it decreases where early compaction removed porosity during lava emplacement. B) Authigenic clay is generally higher in the white sandstone but eogenetic clays in the red sandstone increase toward hot contact. C) Opaque mineral abundance (grain rims and detrital) variability is high in red sandstone, the white sandstone opaque mineral abundance increases toward hot contact, where eogenetic porosity loss prevented bleaching fluid circulation. D) Authigenic calcite is generally higher in white dunes formed during circulation of bleaching fluid, in red dunes calcite increases toward the contact due to volcano-eogenesis. Dune B red clearly shows a decreasing calcite trend away from hot contact, whereas Dune A white calcite remains high and scattered with increasing distance. See Table 3 for T-Test analysis of these data.

Fig. 15. A) $\delta^{13}C$ (PDB) plotted against $\delta^{18}O$ (PDB) for the four samples analyzed, plus two Type 3 contacts from other formerly hot lava-sediment contacts. The calcite fields plotted for comparison are: (1) hydrothermally affected graywacke, Horton et al., (2012); (2) carbonatite, Rollinson (1993); (3) hydrothermal calcite, Dias et al., (2011); (4a, 4b) Entrada Fm hydrocarbon-related, Garden et al., (2001); (5) Navajo and Entrada Fms, Chan et al., (2000); (6) Navajo Fm red cements, Beitler et al., (2005); (7) Permian playa lake, Platt et al., (1994); (8) Namibia Karoo lava-related, Gierlowski-Kordesch et al., (2015); (9) Navajo Fm bleached cements, Beitler et al., (2005); (10) calcretes, Purvis and Wright (1991); (11) modern soil and groundwater carbonates, Europe, Candy et al., (2012); (12) calcrete, Naylor et al., (1989); (13) South Africa calcretes, Solomons et al., (1978); (14) Paraná. calcite geodes, Gilg et al, (2003). Type 2 and Type 3 diagenetic carbonates plot in two distinct populations, with Type 3 red dune carbonate cements having more mantle-like $\delta^{13}C$ values. (B) Modelled calcite $\delta^{18}O$ values in equilibrium with waters of different origins. Calculated meteoric and magmatic fields are shown (using fractionation constants A = -3.39 and B = 2.78, O'Neil et al. 1969) as well as the expected meteoric water, value for Namibia in the Cretaceous (132 Ma). $\delta^{18}O$ values of calcite from our analyses are plotted. NG 28, NG30, and NG34 are from white dunes (Type 2), NG31 is from Type 3 (lava-sediment contact) calcite.

Fig. 16. Map of Dune C. Type 1 and Type 2 diagenesis is separated by a crosscutting N-S-trending dolerite dike.

Fig. 17. Diagram showing the diagenetic evolution of the three sandstone types discussed. Type 3 diagenesis is labelled (3) and includes both red and white sandstones. The red (Type 1) sandstone is depicted by the red lines, and the white (Type 2) sandstone by the blue lines. After initial burial by lava the diagenetic pathways diverge and are labelled (1) for Type 1 diagenesis and (2) for Type 2 diagenesis.

Fig. 18. Conceptual model of fluid flow through Dune Valley as controlled by igneous rocks. A) Dolerite dikes acting as barriers to horizontal fluid flow. B) Lateral fluid flow permitted through sandstone and basalt. C) Multidirectional flow permitted through sandstone. Diagram is not to scale.

Appendix 1. Point-count data (500 points), and permeability data (nitrogen probe) presented for all red and white dunes sampled. *Repeat section.

Appendix. 2. XRF Major element data for isolated-dune samples

Appendix. 3. Stable-isotope data for calcite in sandstone samples analyzed.

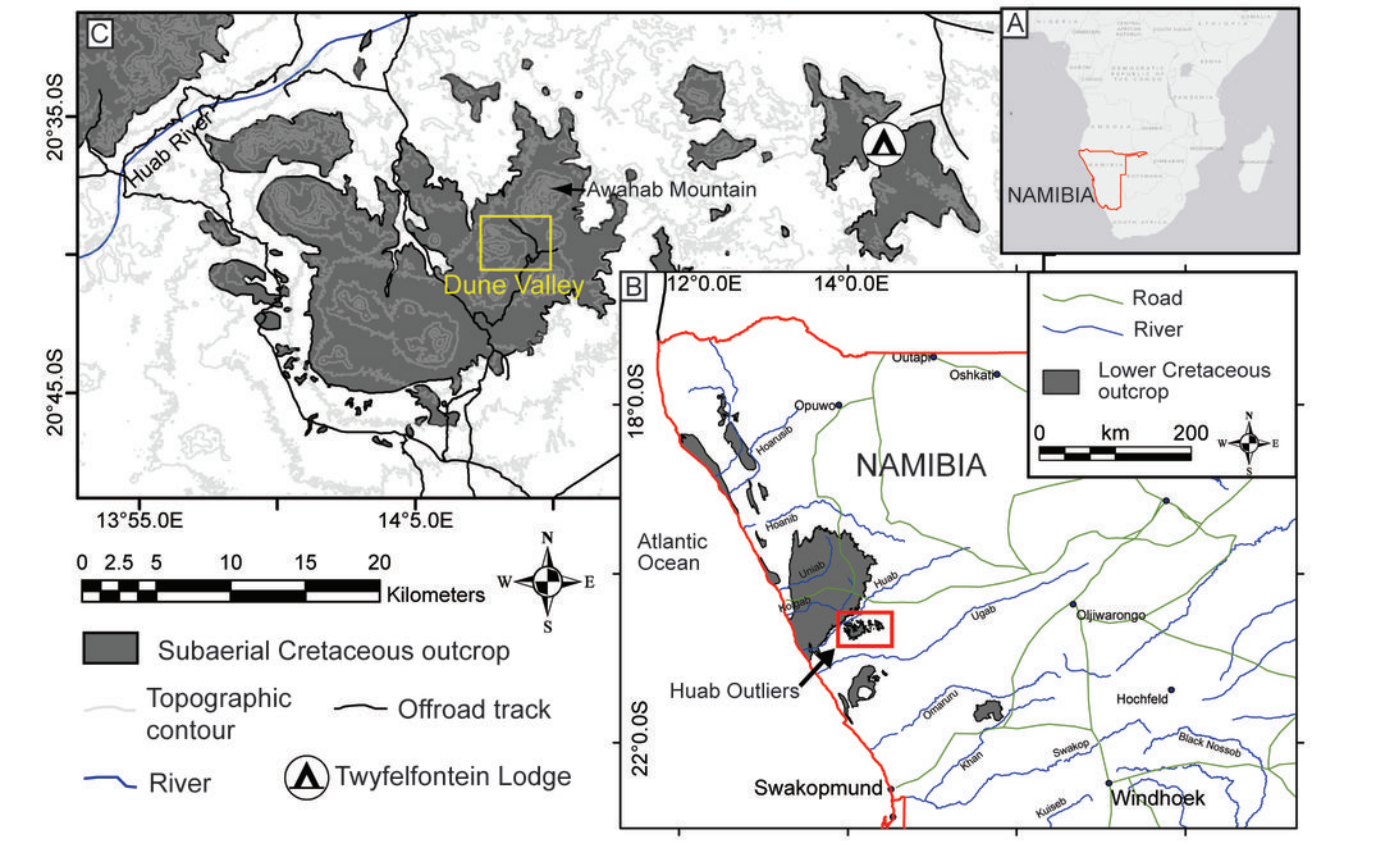
C
20°35.0S
20°45.0S
13°55.0E
14°5.0E
Huab River
Awahab Mountain
Dune Valley
A
NAMIBIA
B
12°0.0E
14°0.0E
18°0.0S
22°0.0S
Road
River
Lower Cretaceous outcrop
0 km 200
N
W
E
S
NAMIBIA
Atlantic Ocean
Outapi
Oshkati
Opuwo
Hoarusib
Hoanib
Uniab
Huab
Koigab
Ugab
Huab Outliers
Omaruru
Khan
Swakop
Kuiseb
Swakopmund
Windhoek
Otjiwarongo
Hochfeld
Black Nossob
0 2.5 5 10 15 20
Kilometers
Subaerial Cretaceous outcrop
Topographic contour
Offroad track
River
Twyfelfontein Lodge

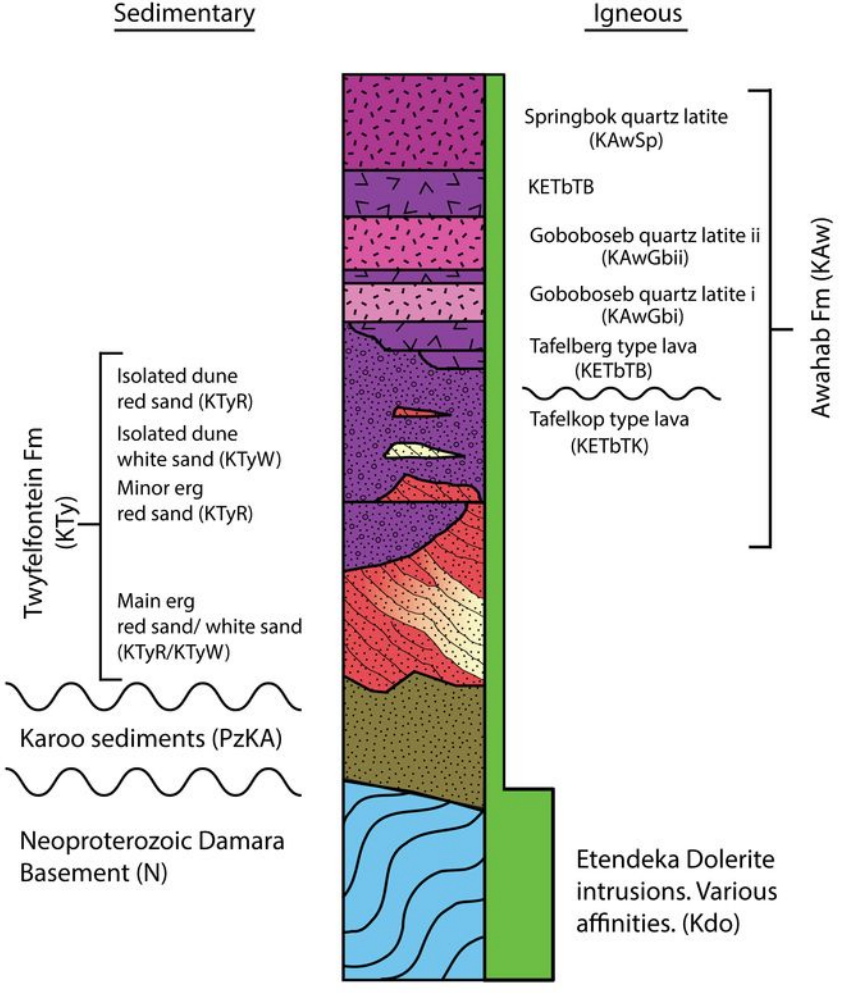
Sedimentary
Igneous
Springbok quartz latite
(KAwSp)
KETbTB
Goboboseb quartz latite ii
(KAwGbii)
Goboboseb quartz latite i
(KAwGbi)
Tafelberg type lava
(KETbTB)
Tafelkop type lava
(KETbTK)
Awahab Fm (KAw)
Twyfelfontein Fm
(KTy)
Isolated dune
red sand (KTyR)
Isolated dune
white sand (KTyW)
Minor erg
red sand (KTyR)
Main erg
red sand/ white sand
(KTyR/KTyW)
Karoo sediments (PzKA)
Neoproterozoic Damara
Basement (N)
Etendeka Dolerite
intrusions. Various
affinities. (Kdo)

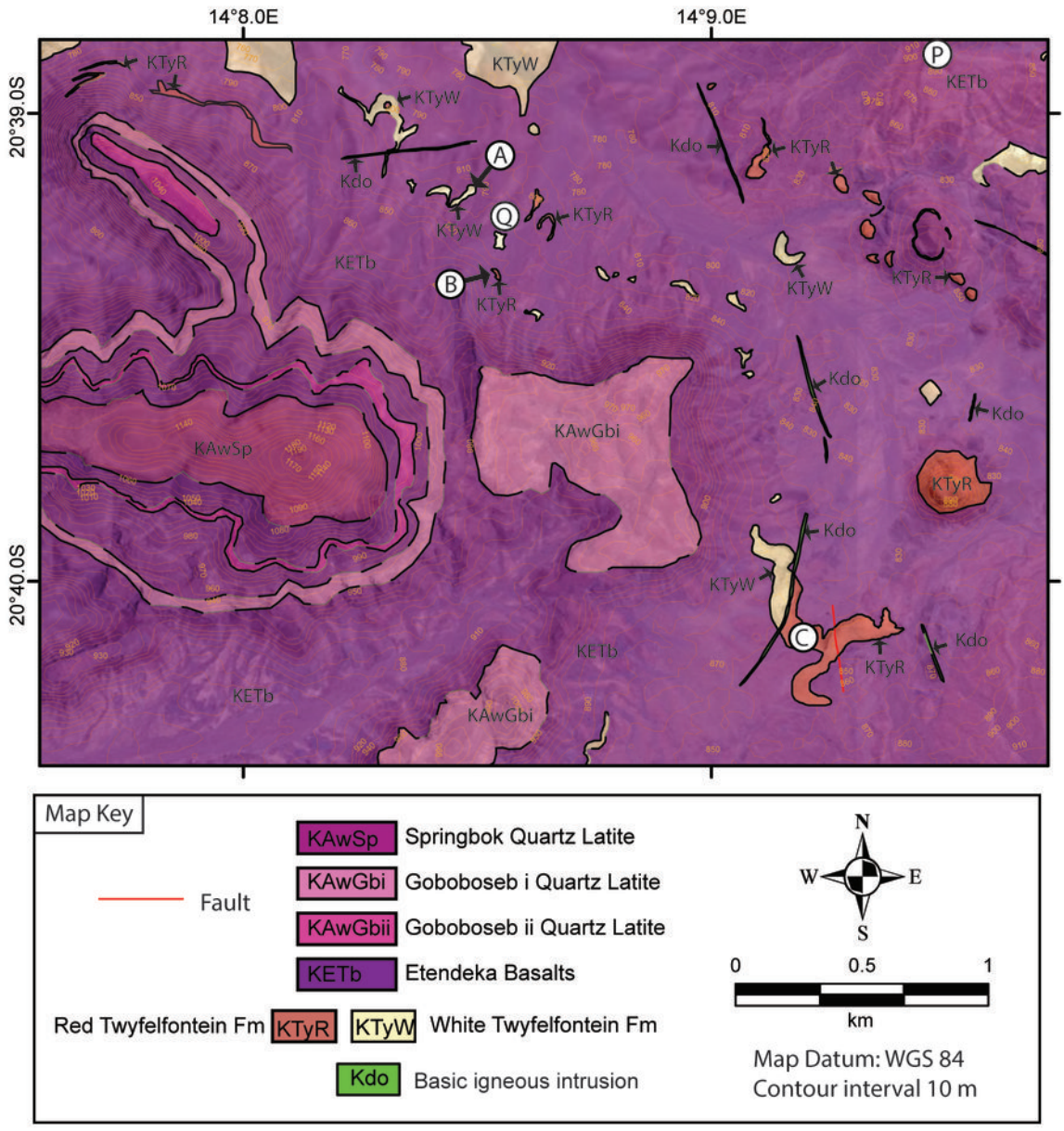
14°8.0E
14°9.0E
20°39.0S
20°40.0S
KTyR
KTyW
KTyW
Kdo
A
KTyW
Q
KTyR
KETb
B
KTyR
KAwSp
KAwGbi
KETb
KAwGbi
KETb
Kdo
KTyR
P
KETb
Kdo
KTyR
KTyW
KTyR
Kdo
Kdo
KTyR
Kdo
KTyW
C
KTyR
Kdo
Map Key
KAwSp
Springbok Quartz Latite
KAwGbi
Goboboseb i Quartz Latite
KAwGbii
Goboboseb ii Quartz Latite
KETb
Etendeka Basalts
Fault
Red Twyfelfontein Fm
KTyR
KTyW
White Twyfelfontein Fm
Kdo
Basic igneous intrusion
N
W
E
S
0
0.5
1
km
Map Datum: WGS 84
Contour interval 10 m

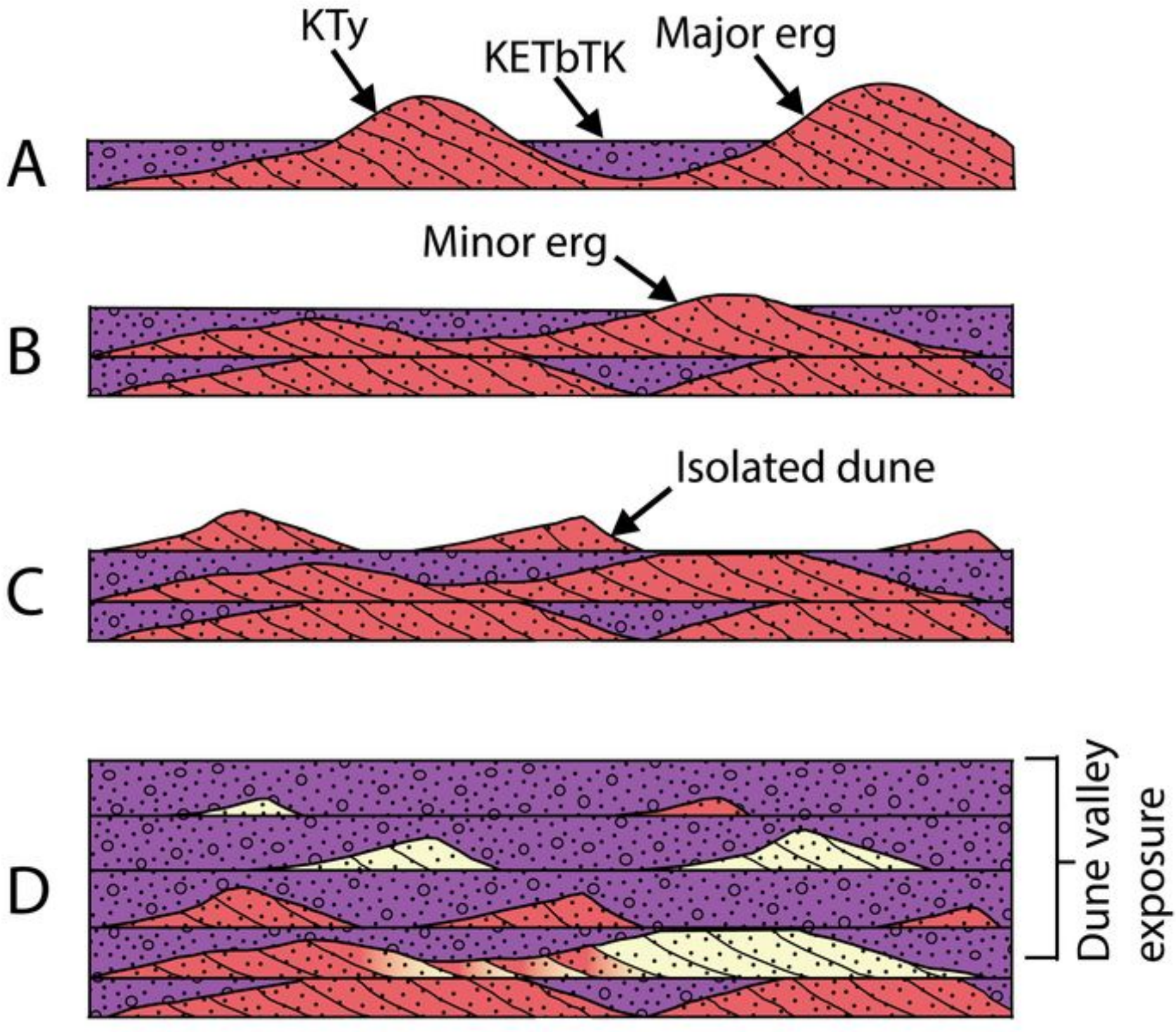
KTy
KETbTK
Major erg
A
Minor erg
B
Isolated dune
C
D
Dune valley
exposure

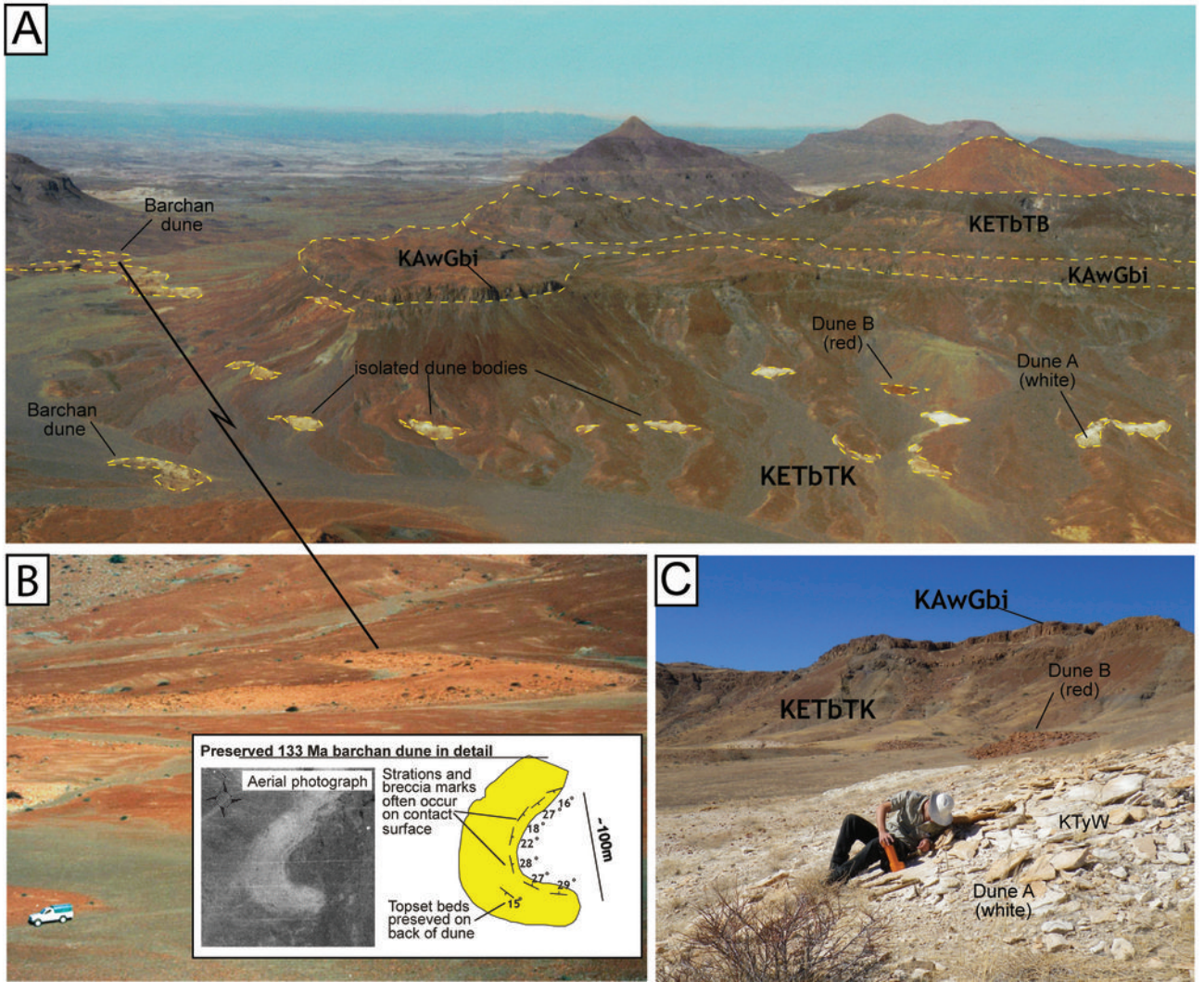
A
Barchan dune
KAwGbi
KETbTB
KAwGbi
Dune B (red)
Dune A (white)
isolated dune bodies
Barchan dune
KETbTK
B
Preserved 133 Ma barchan dune in detail
Aerial photograph
Strations and breccia marks often occur on contact surface
16°
27°
18°
22°
28°
27°
29°
15°
~100m
Topset beds preseved on back of dune
C
KAwGbi
Dune B (red)
KETbTK
KTyW
Dune A (white)

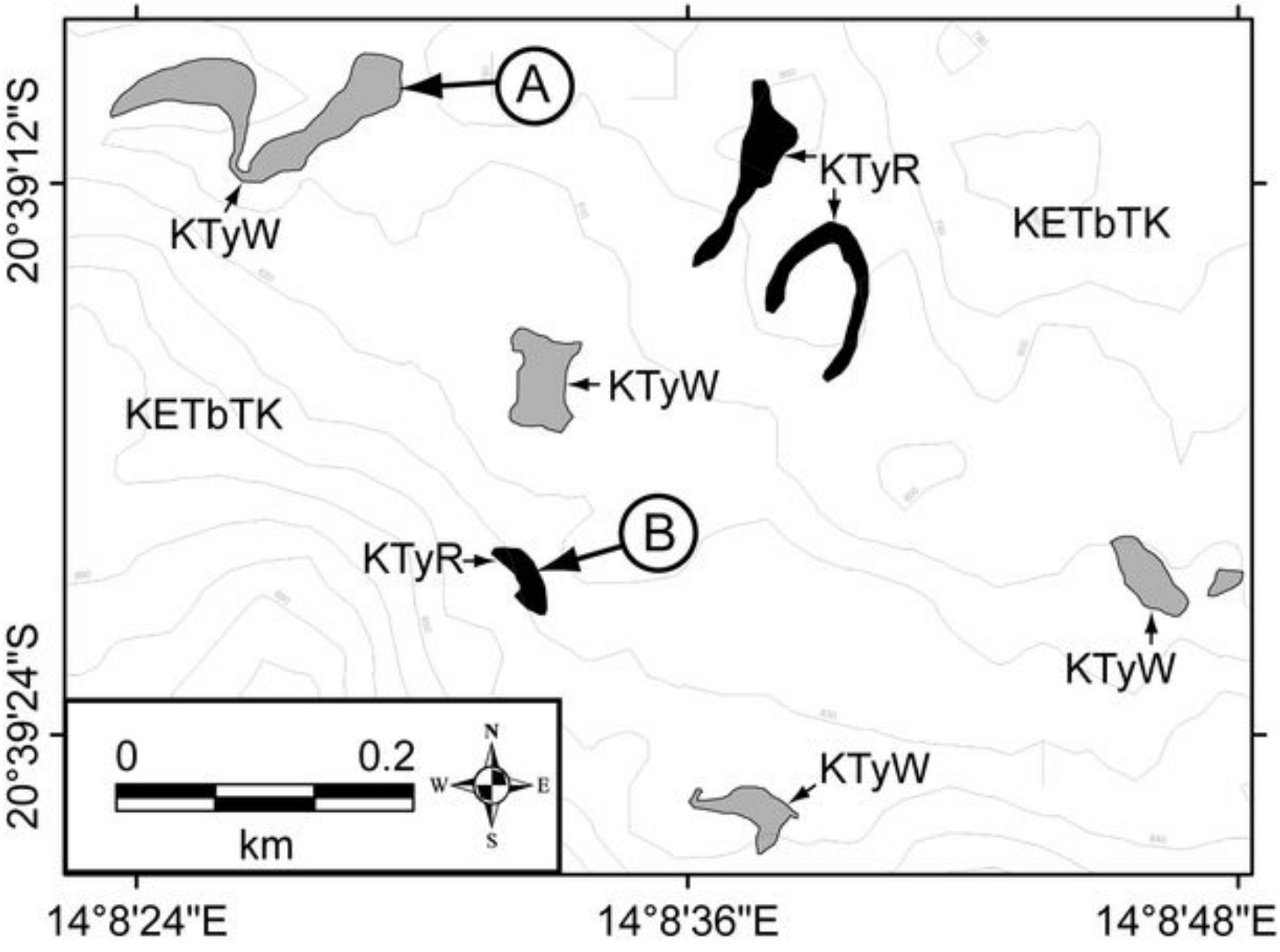
20°39'12"S
20°39'24"S
14°8'24"E
14°8'36"E
14°8'48"E
A
B
KTyW
KTyR
KETbTK
KTyW
KETbTK
KTyR
KTyW
KTyW
0
0.2
km
N
W
E
S

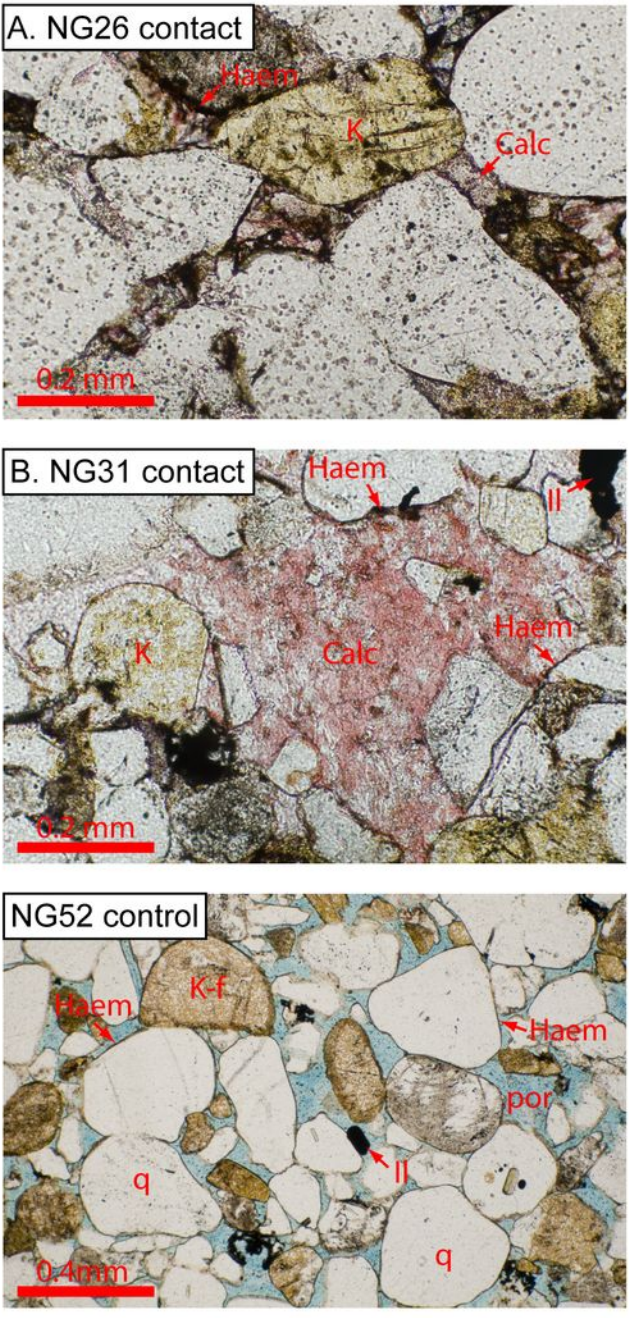
A. NG26 contact
Haem
K
Calc
0.2mm
B. NG31 contact
Haem
Il
K
Calc
Haem
0.2mm
NG52 control
Haem
K-f
Haem
por
Il
q
q
0.4mm

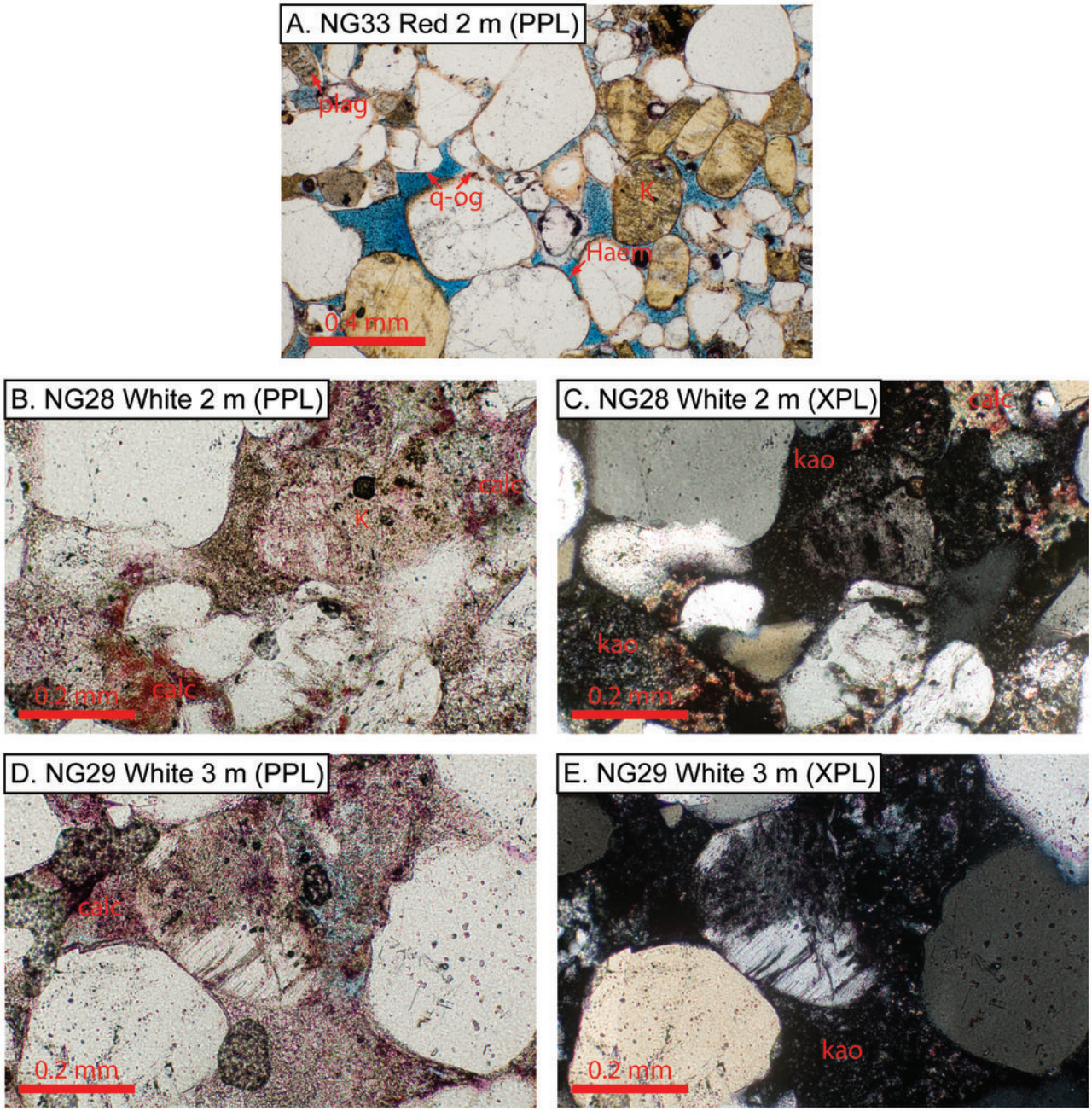
A. NG33 Red 2 m (PPL)
plag
q-og
K
Haem
0.4 mm
B. NG28 White 2 m (PPL)
calc
K
0.2 mm
calc
C. NG28 White 2 m (XPL)
calc
kao
kao
0.2 mm
D. NG29 White 3 m (PPL)
calc
0.2 mm
E. NG29 White 3 m (XPL)
kao
0.2 mm

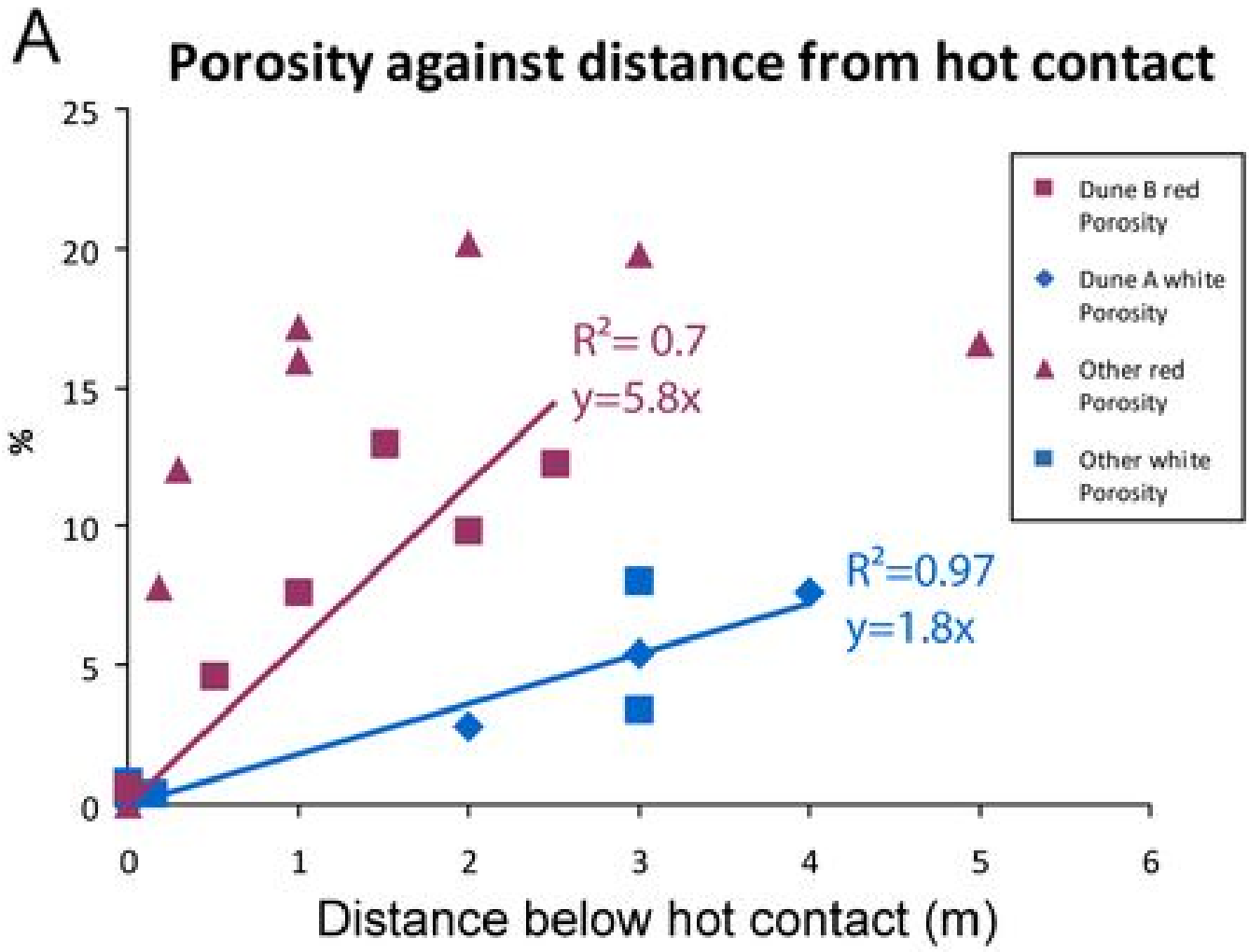
A
Porosity against distance from hot contact
25
20
15
10
5
0
%
0
1
2
3
4
5
6
Distance below hot contact (m)
R²= 0.7
y=5.8x
R²=0.97
y=1.8x
Dune B red Porosity
Dune A white Porosity
Other red Porosity
Other white Porosity

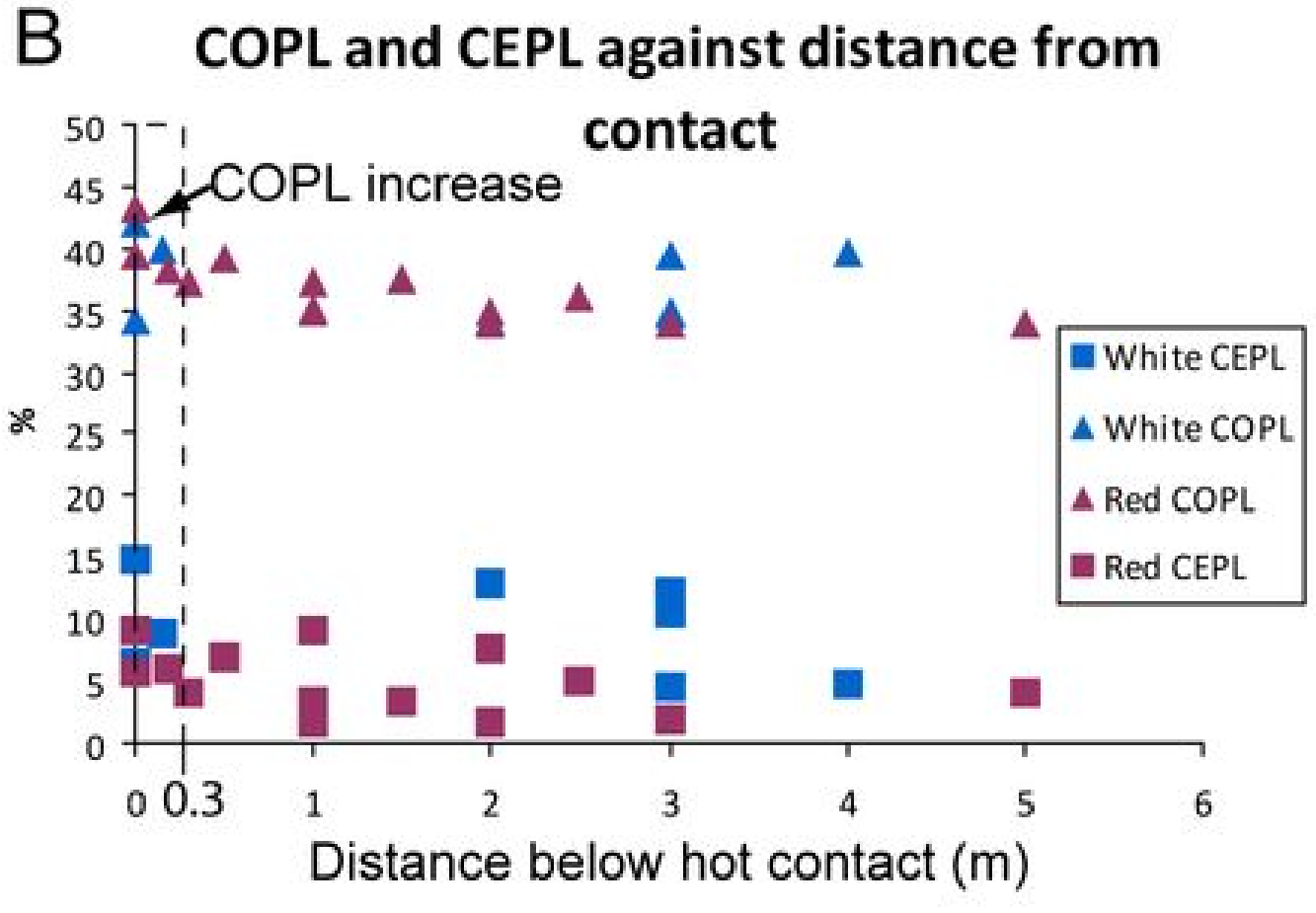
B
COPL and CEPL against distance from contact
50
45
40
35
30
25
20
15
10
5
0
%
COPL increase
0
0.3
1
2
3
4
5
6
Distance below hot contact (m)
White CEPL
White COPL
Red COPL
Red CEPL

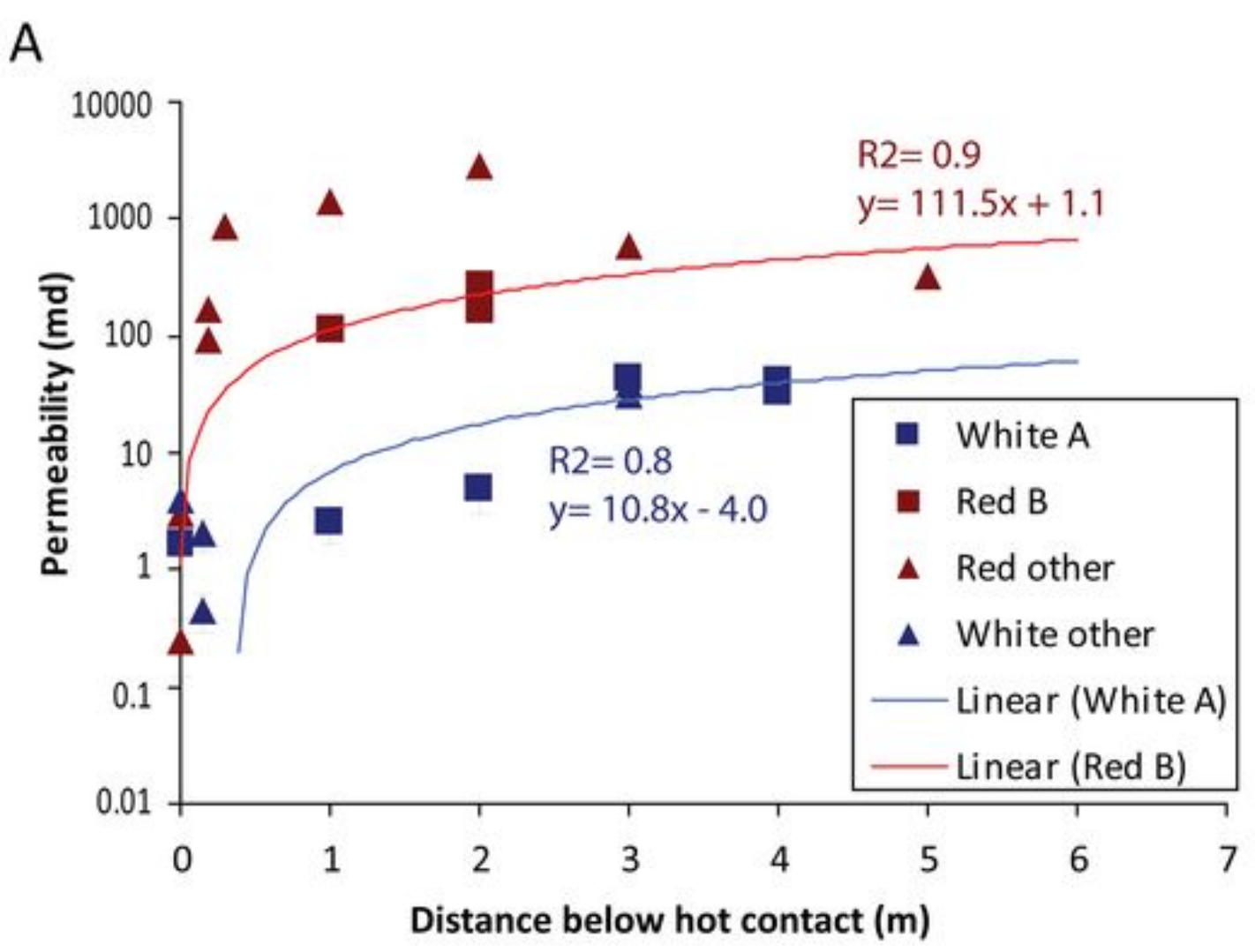
A
10000
1000
100
10
1
0.1
0.01
Permeability (md)
R2= 0.9
y= 111.5x + 1.1
R2= 0.8
y= 10.8x - 4.0
White A
Red B
Red other
White other
Linear (White A)
Linear (Red B)
0
1
2
3
4
5
6
7
Distance below hot contact (m)

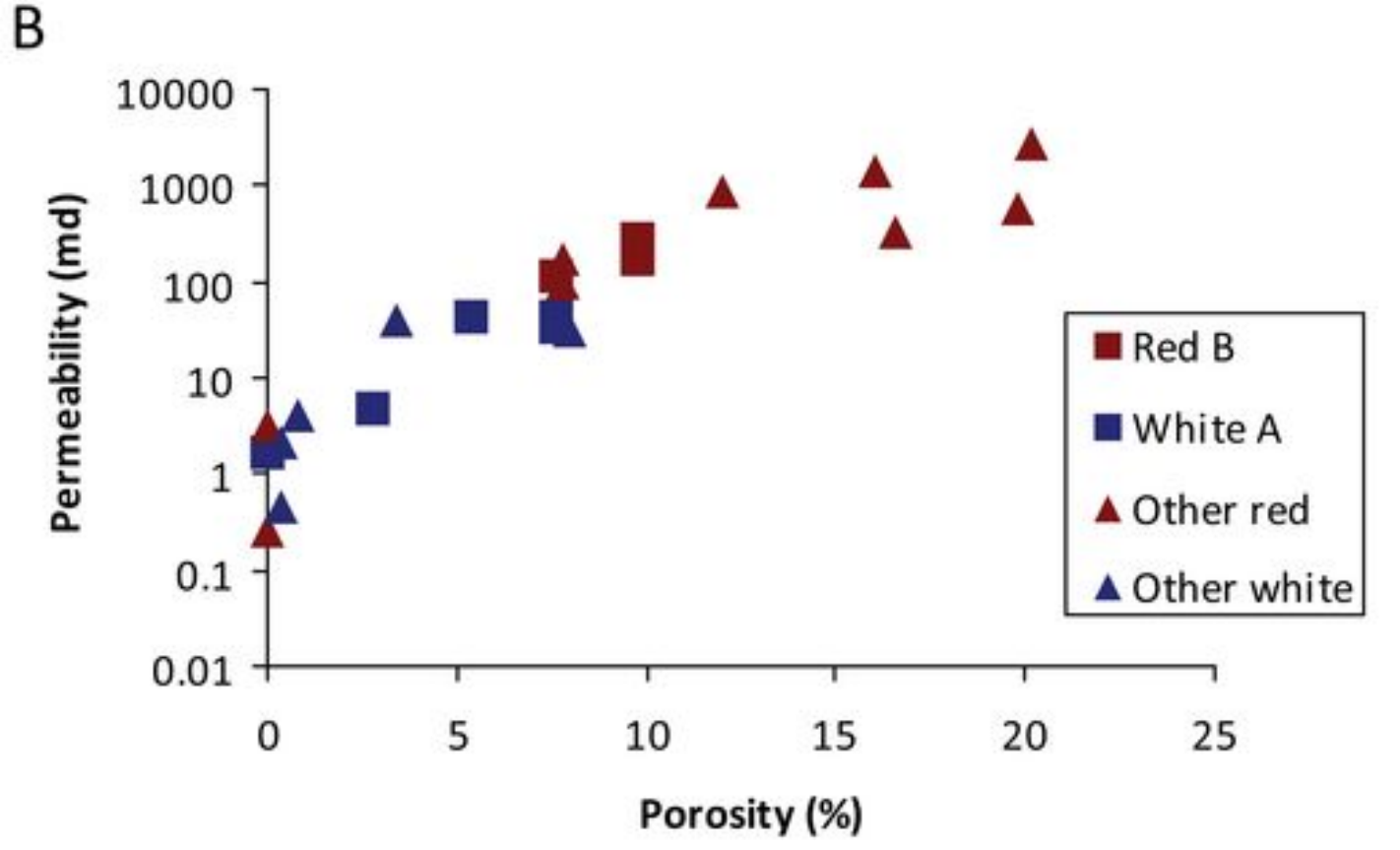
B
10000
1000
100
10
1
0.1
0.01
Permeability (md)
Red B
White A
Other red
Other white
0
5
10
15
20
25
Porosity (%)

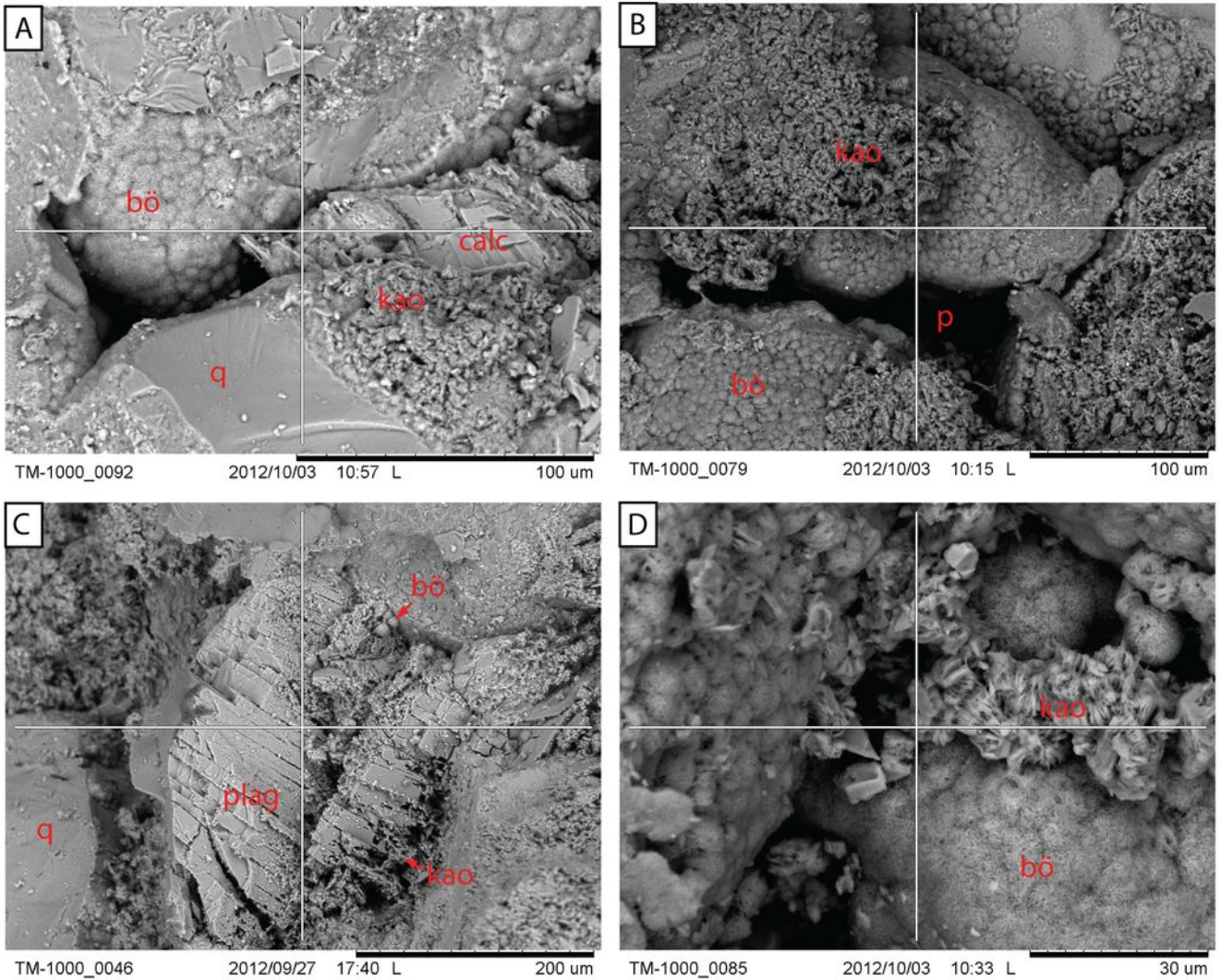
A
bö
calc
kao
q
TM-1000_0092 2012/10/03 10:57 L 100 um
B
kao
p
bö
TM-1000_0079 2012/10/03 10:15 L 100 um
C
bö
plag
q
kao
TM-1000_0046 2012/09/27 17:40 L 200 um
D
kao
bö
TM-1000_0085 2012/10/03 10:33 L 30 um

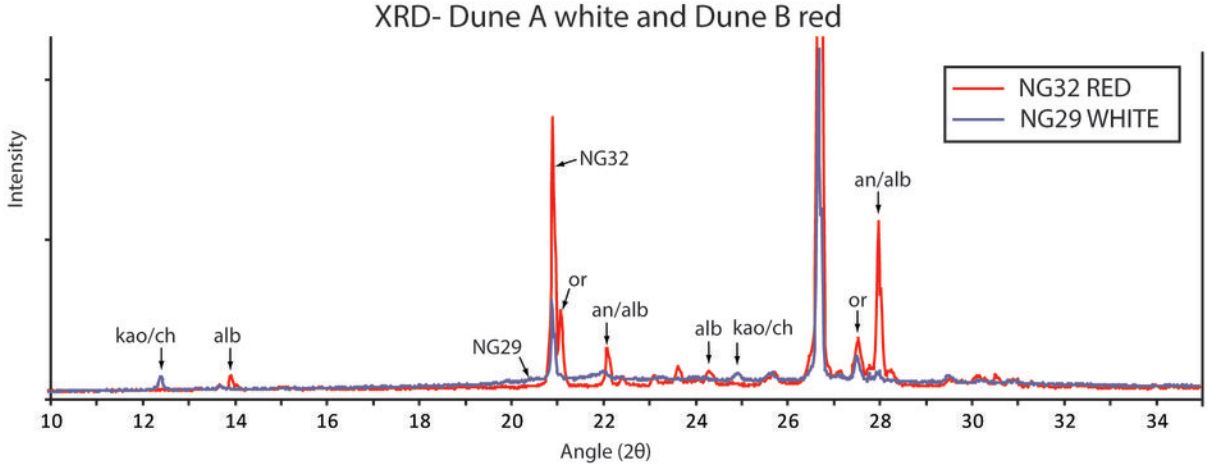
XRD- Dune A white and Dune B red
NG32 RED
NG29 WHITE
Intensity
NG32
an/alb
or
an/alb
or
kao/ch
alb
NG29
alb
kao/ch
10
12
14
16
18
20
22
24
26
28
30
32
34
Angle (2θ)

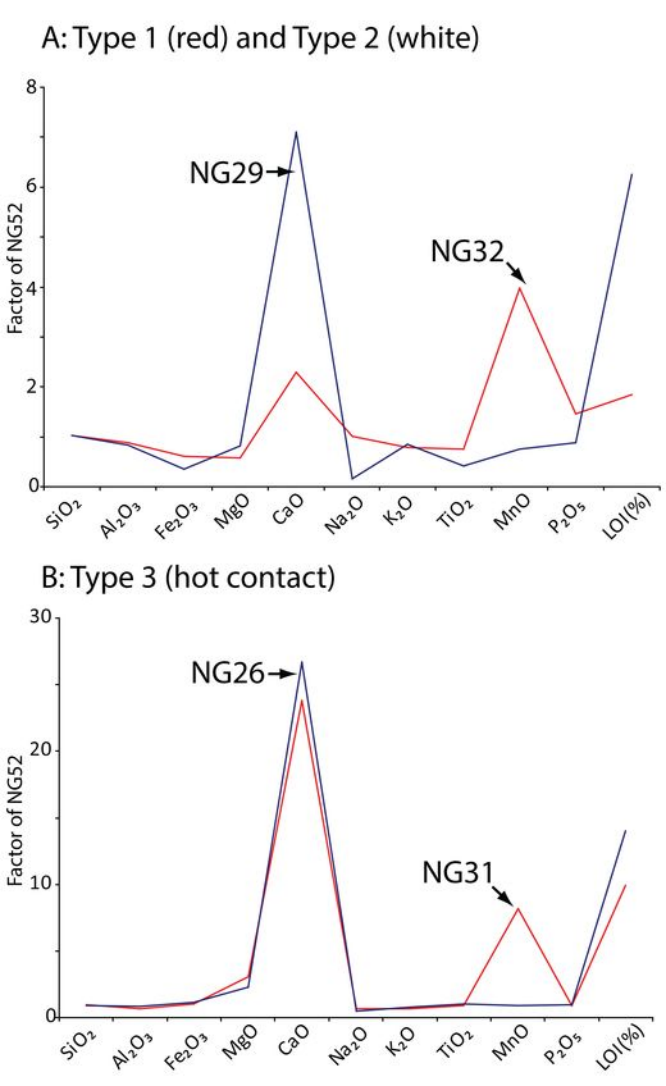
A: Type 1 (red) and Type 2 (white)
Factor of NG52
8
6
4
2
0
NG29
NG32
SiO2
Al2O3
Fe2O3
MgO
CaO
Na2O
K2O
TiO2
MnO
P2O5
LOI(%)
B: Type 3 (hot contact)
Factor of NG52
30
20
10
0
NG26
NG31
SiO2
Al2O3
Fe2O3
MgO
CaO
Na2O
K2O
TiO2
MnO
P2O5
LOI(%)

A: Authigenic Quartz

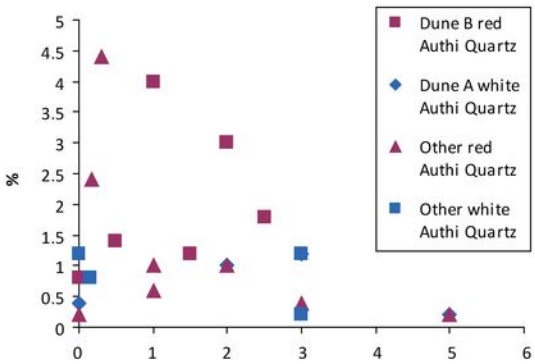

B: Authigenic Clay

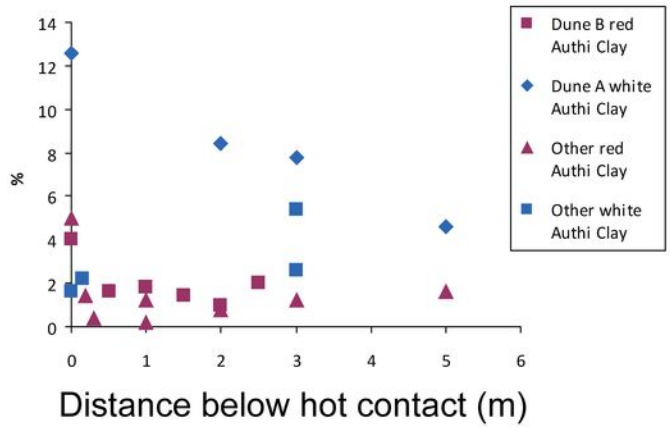

C: Opaques

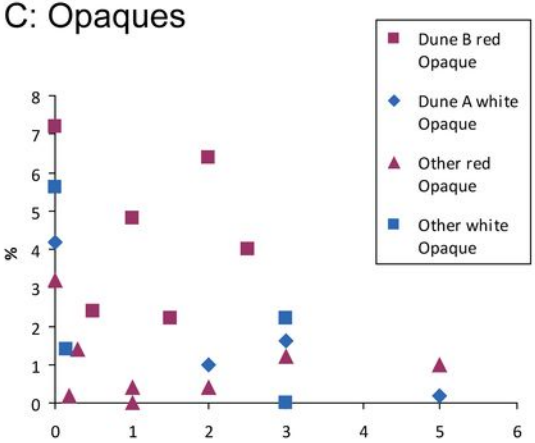

D: Authigenic Calcite

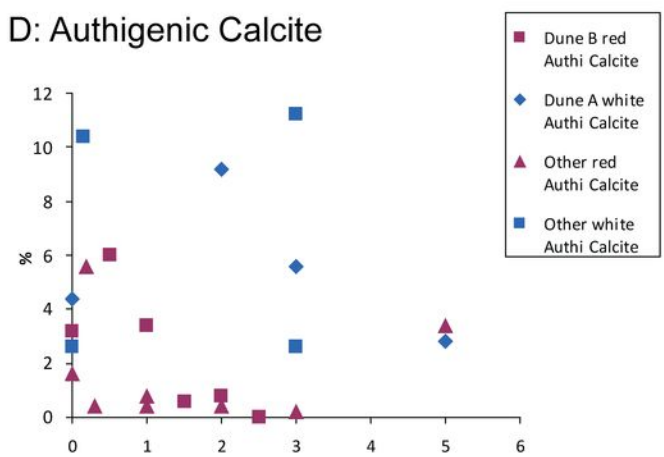

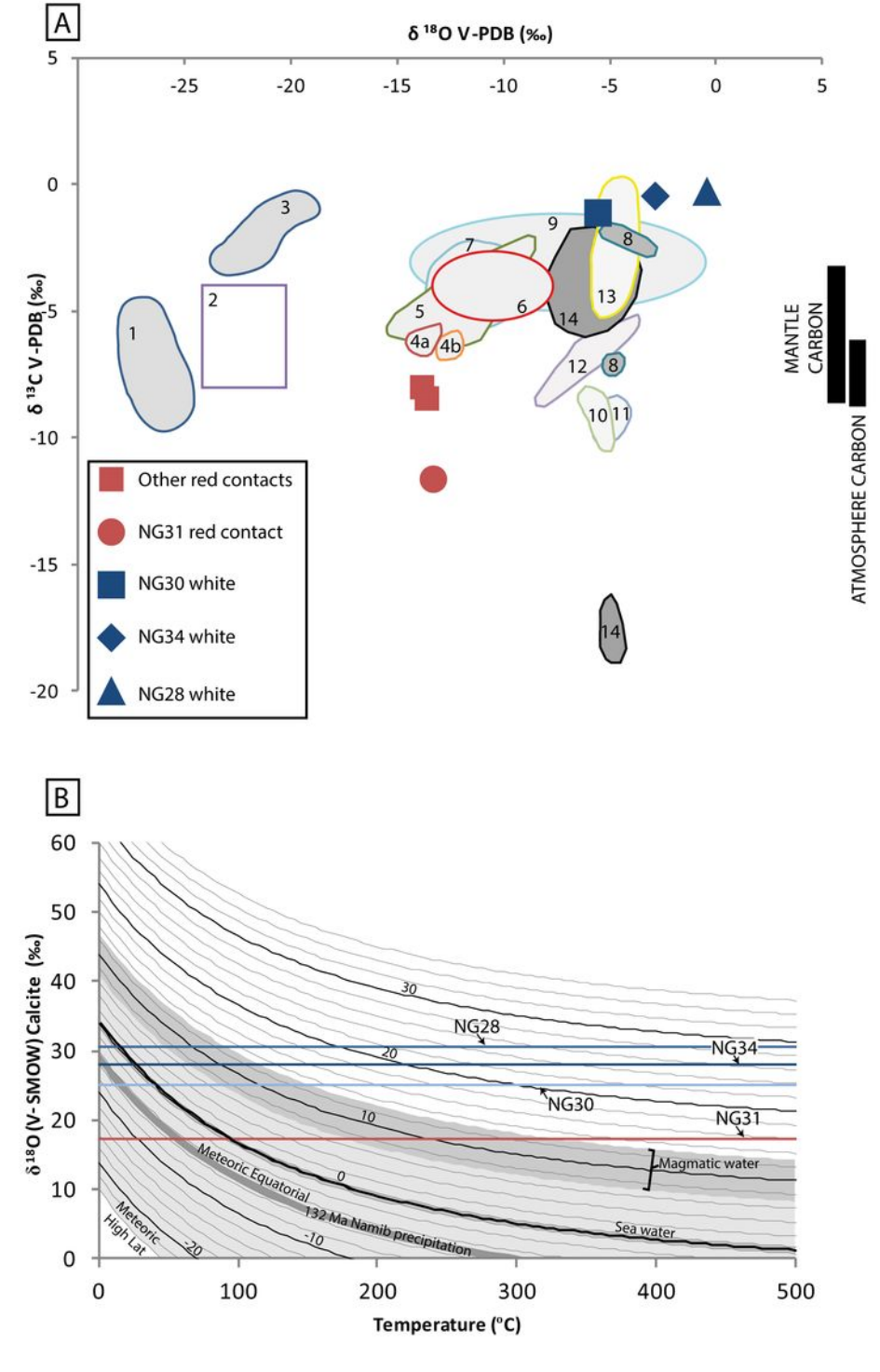
A
δ 18O V-PDB (‰)
δ 13C V-PDB (‰)
MANTLE CARBON
ATMOSPHERE CARBON
Other red contacts
NG31 red contact
NG30 white
NG34 white
NG28 white
B
δ18O (V- SMOW) Calcite (‰)
Temperature (°C)
NG28
NG34
NG30
NG31
Magmatic water
Meteoric Equatorial
132 Ma Namib precipitation
Sea water
Meteoric High Lat

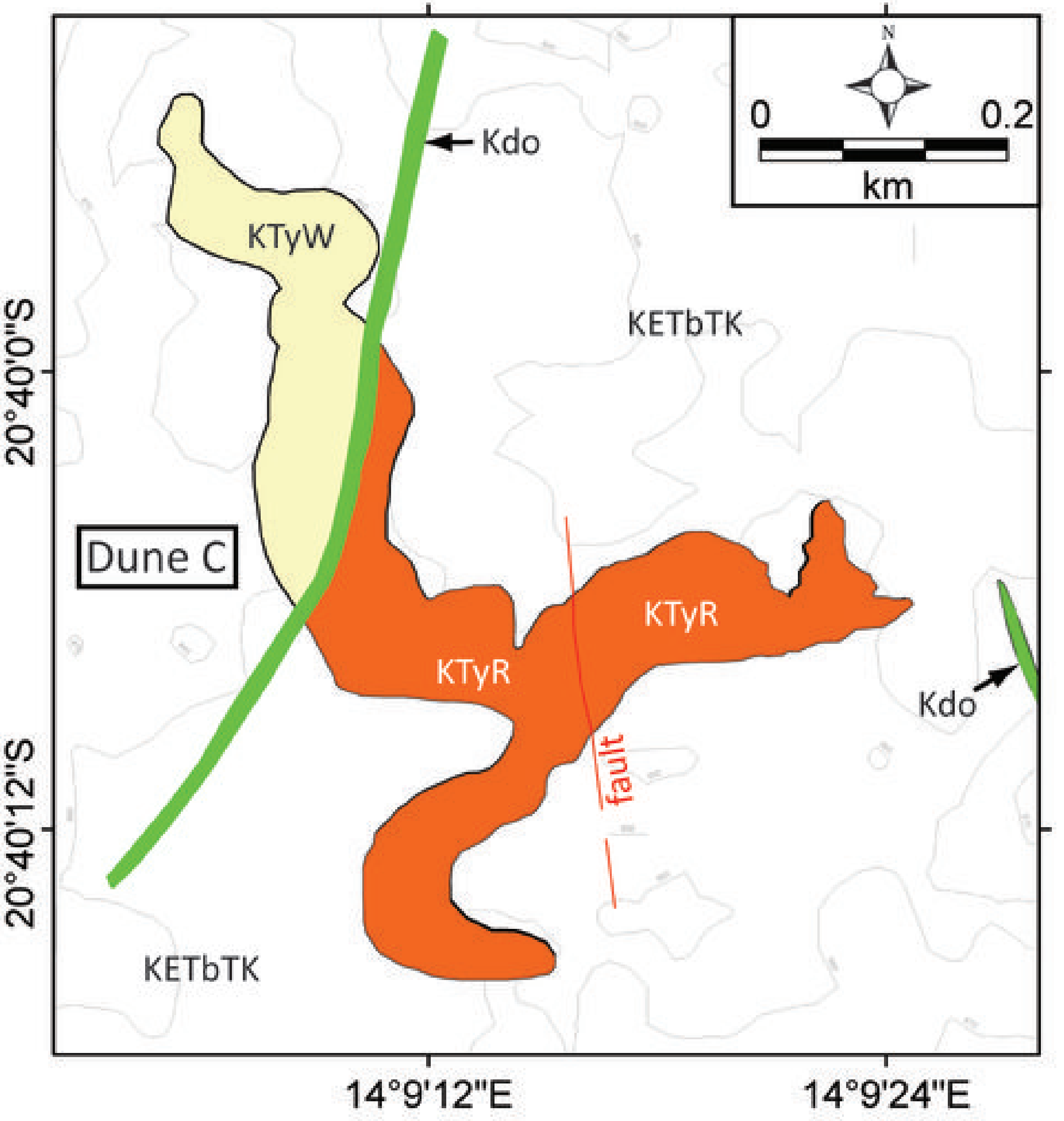
N
0
0.2
km
Kdo
KTyW
KETbTK
Dune C
KTyR
KTyR
fault
Kdo
KETbTK
20°40'0"S
20°40'12"S
14°9'12"E
14°9'24"E

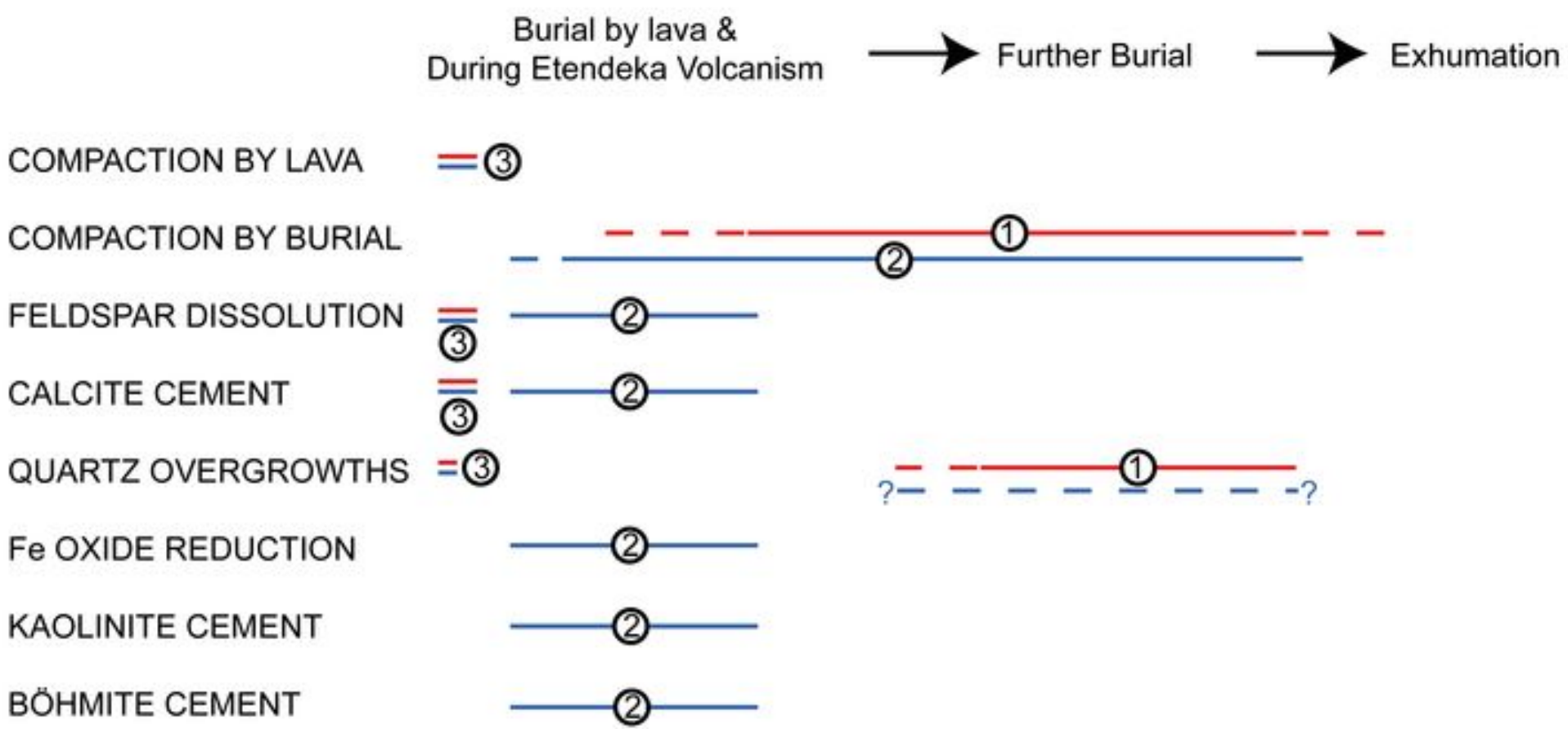
Burial by lava &
During Etendeka Volcanism
Further Burial
Exhumation
COMPACTION BY LAVA
COMPACTION BY BURIAL
FELDSPAR DISSOLUTION
CALCITE CEMENT
QUARTZ OVERGROWTHS
Fe OXIDE REDUCTION
KAOLINITE CEMENT
BÖHMITE CEMENT
1
2
3
?
?

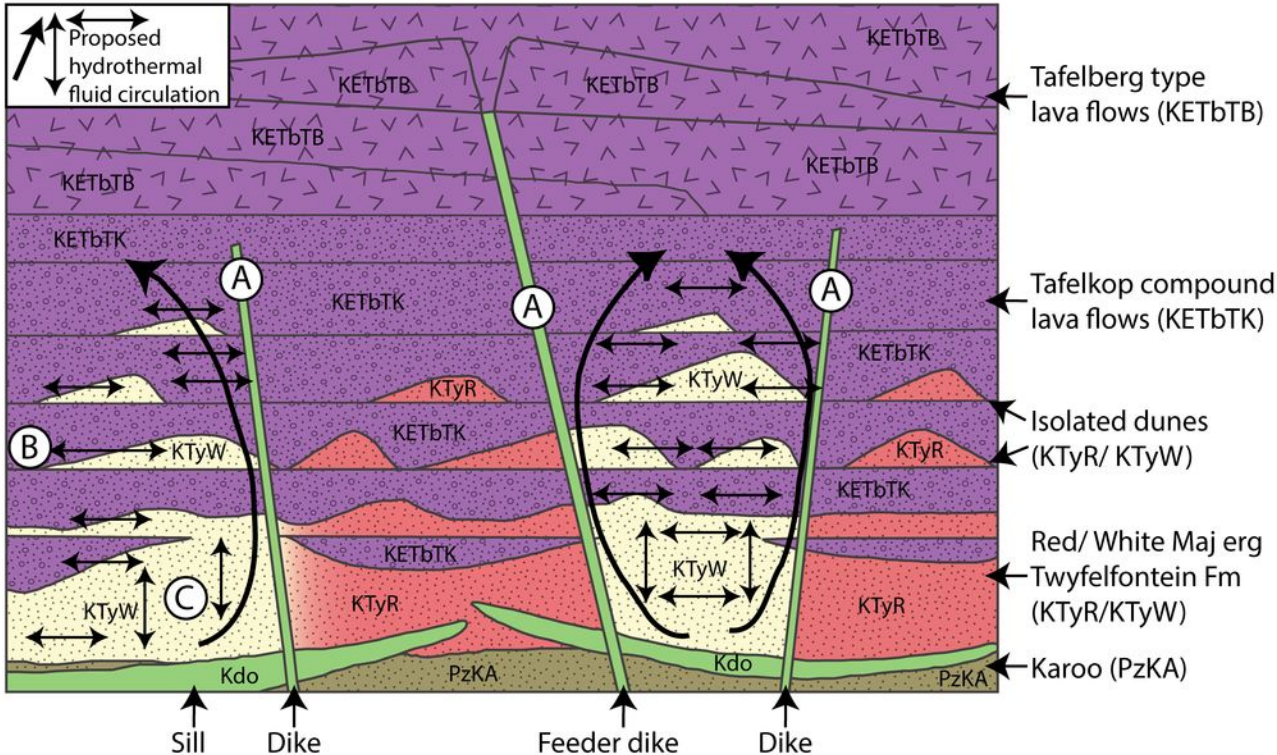
Proposed hydrothermal fluid circulation
KETbTB
KETbTK
KTyR
KTyW
Kdo
PzKA
A
B
C
Sill
Dike
Feeder dike
Dike
Tafelberg type lava flows (KETbTB)
Tafelkop compound lava flows (KETbTK)
Isolated dunes (KTyR/ KTyW)
Red/ White Maj erg Twyfelfontein Fm (KTyR/KTyW)
Karoo (PzKA)

Table. 1. Average point-counting data for each “type” of diagenesis identified in this study. 500 points were counted for each sample.

Case	NG52 Red Control	Red (average)	White (average)	Contact (average)
Diagenesis	Type 1	Type 1	Type 2	Type 3
Distance below lava (m)	NA	2.0	2.7	0.2
Quartz %	55.2	50.0	60.4	54.9
K-Spar %	20.6	22.3	14.4	22.7
Plag %	7.4	6.5	4.1	5.3
Lithic %	1.2	0.6	0.6	0.8
Authi-Calcite %	0.0	0.8	5.9	4.7
Authi-Clay %	1.2	1.1	7.6	3.8
Authi-Q %	0.0	1.5	0.7	1.4
Authi-feldspar %	0.0	0.1	0.0	0.1
Porosity %	12.4	15.2	4.8	2.7
Opaque %	2.0	1.9	1.4	3.6
Fluorite %	0.0	0.2	0.1	0.0
Detrital Amphibole %	0.0	0.0	0.0	0.0
Zeolite %	0.0	0.0	0.1	0.0
Pmc	15.6	20.8	20.5	16.3
COPL %	39.6	35.6	35.7	38.9
CEPL %	7.5	3.6	10.3	8.4
ICOMPACT	0.8	0.9	0.8	0.8
Probe Permeability md	1747.4	1094.6	25.9	31.1

Table. 2. Petrological and mineralogical comparison of contact sediments at Dune A white and Dune B red.

Data type	**Dune A white contact (NG 26)**	**Dune B red contact (NG31)**	**Control (NG52)**
Petrographical	Highly compacted, feldspars altering to clays, pokilitic calcite cement	Highly compacted, feldspars altering to clays, pokilitic calcite cement	Compacted, low amount of alteration of detrital grains, pores and throats open. Cements absent.
XRD (authigenic in brackets)	Quartz, orthoclase, anorthite, albite, (calcite), (clinochlore or kaolinite)	Quartz, orthoclase, anorthite, albite, ilmenite, (calcite), (fluorite, weak), (clinochlore or kaolinite, weak)	Quartz, orthoclase, anorthite, albite, (iron minerals, weak peaks)

Table. 3. T-Test results of the point counting and permeability analysis of Type 1 red dunes and Type 2 white dunes. All parameters other than opaque minerals have a T-Test result showing that the phase counted is either statistically significantly different (95%) or highly statistically significantly different (99%). The opaque-mineral result supports the hypothesis that iron oxides are reprecipitated locally as nodules. Highly statistically significant results are appended with an asterisk.

Parameter	**Probability different**	**Statistically significant**
Porosity	0.001	YES*
Permeability	0.013	YES
Authigenic quartz	0.046	YES
Authigenic calcite	0.048	YES
Clay	<0.001	YES*
Opaque minerals	0.411	NO